The antigenic landscape of human influenza N2 neuraminidases from 2009 until 2017

João Paulo Portela Catani[1,2], Anouk Smet[1,2], Tine Ysenbaert[1,2], Marnik Vuylsteke[3], Guy Bottu[4], Janick Mathys[4], Alexander Botzki[4], Guadalupe Cortes-Garcia[5], Tod Strugnell[5], Raul Gomila[5], John Hamberger[5], John Catalan[5], Irina V. Ustyugova[5], Timothy Farrell[5], Svetlana Stegalkina[5], Satyajit Ray[5], Lauren LaRue[5], Xavier Saelens[1,2*], Thorsten U. Vogel[5*]

[1]VIB Center for Medical Biotechnology, VIB, B-9052 Ghent, Belgium

[2]Department of Biochemistry and Microbiology, Ghent University, B-9052 Ghent, Belgium

[3]Gnomixx, Melle, Belgium

[4]VIB Bioinformatics Core, VIB, B-9052 Ghent, Belgium

[5]Sanofi, Research North America, Cambridge, Massachusetts, USA

* Corresponding authors:

E-mail: Xavier.saelens@vib-ugent.be and Thorsten.Vogel@sanofi.com

Abstract

Human H3N2 influenza viruses are subject to rapid antigenic evolution which translates into frequent updates of the composition of seasonal influenza vaccines. Despite these updates, the effectiveness of influenza vaccines against H3N2-associated disease is suboptimal. Seasonal influenza vaccines primarily induce hemagglutinin-specific antibody responses. However, antibodies directed against influenza neuraminidase (NA) also contribute to protection. Here, we analyzed the antigenic diversity of a panel of N2 NAs derived from human H3N2 viruses that circulated between 2009 and 2017. The antigenic breadth of these NAs was determined based on the NA inhibition (NAI) of a broad panel of ferret and mouse immune sera that were raised by infection and recombinant N2 NA immunization. This assessment allowed us to distinguish at least 4 antigenic groups in the N2 NAs derived from human H3N2 viruses that circulated between 2009 and 2017. Computational analysis further revealed that the amino acid residues in N2 NA that have a major impact on susceptibility to NAI by immune sera are in proximity of the catalytic site. Finally, a machine learning method was developed that allowed to accurately predict the impact of mutations that are present in our N2 NA panel on NAI. These findings have important implications for the renewed interest to develop improved influenza vaccines based on the inclusion of a protective NA antigen formulation.

43 **Introduction**

44 Neuraminidase (NA) and hemagglutinin (HA) constitute the two major antigenic proteins at the
45 surface of influenza A and B virions (Uyeki et al., 2022). While HA mediates binding to sialic acids and
46 membrane fusion, NA catalyses the removal of sialic acid residues from sialylated glycoproteins and
47 glycolipids. This complementary role of HA and NA enables influenza virions to penetrate the mucus
48 barrier that lines the respiratory epithelium and newly formed virions to be released from the infected
49 cell (de Vries et al., 2020; Matrosovich et al., 2004; Palese et al., 1974). Immunity against influenza is
50 associated with the presence of anti-HA antibodies in serum, as determined by a hemagglutination
51 inhibition assay. In line with this, the composition of licensed influenza vaccines is primarily focused
52 on the antigenic characteristics of HA as the protective vaccine antigen (Cox, 2013). Multiple studies,
53 however, have underscored the protective potential of anti-NA immune responses as determined by
54 NA inhibition (NAI) assays (Couch et al., 2013; Maier et al., 2019; Memoli et al., 2016; Monto and
55 Kendal, 1973; Monto et al., 2015; Ng et al., 2019; Weiss et al., 2019). There is also evidence that pre-
56 existing anti-N2 immunity induced by prior exposure to H2N2 viruses that circulated in the population
57 from 1957 to 1968, tempered the impact of the H3N2 pandemic virus that emerged in 1968 (Eickhoff
58 and Meiklejohn, 1969; Jester et al., 2020; Monto and Kendal, 1973; Viboud et al., 2005). Further, the
59 pharmacological inhibition of NA activity is a well-established therapeutic strategy to try to reduce
60 influenza severity and duration (Leneva et al., 2000; Yen et al., 2005). In addition, antibodies with NAI
61 activity can protect against influenza virus infection in pre-clinical models (Chen et al., 2018; Deroo et
62 al., 1996; Rosu et al., 2022; Wan et al., 2018; Wohlbold et al., 2017).

63 Since its appearance in 1968, human H3N2 viruses have been evolving faster than the co-circulating
64 H1N1 and influenza B viruses (Bedford et al., 2014; Potter et al., 2019). The overall Influenza virus
65 vaccine effectiveness varies between seasons and, despite frequent updates of the H3N2 HA
66 component, the effectiveness of influenza vaccines against H3N2-associated disease ranges between
67 5 and 39%, which is lower than the effectiveness against H1N1 and influenza B (Belongia et al., 2016).
68 In this context the use of NA as a complementary vaccine antigen might improve influenza vaccine
69 effectiveness, for example by compensating for HA-based antigenic mismatches in circulating
70 influenza virus strains (Krammer et al., 2018).

71 Phylogenetic analyses of HA and NA genes of human H3N2 viruses revealed the asynchronous
72 evolution of the 2 proteins. In addition, the evolutionary rate as determined by the accumulation of
73 mutations over time, is estimated to be 1.5 times lower for NA than for HA (Westgeest et al., 2012).
74 Despite the strong evidence that immune responses directed against NA can contribute to protection
75 against influenza, a comprehensive insight in the antigenic breadth and evolution of the H3N2 NA

antigen is lacking (Nachbagauer et al., 2017; Rajendran et al., 2017; Smith et al., 2004; Westgeest et al., 2012).

Here, we determined the antigenic landscape of N2 NAs derived from human H3N2 strains that were isolated between 2009 and 2017. This analysis allowed the identification of at least 4 N2 NA antigenic groups and to estimate the weight of amino acid changes on their contribution to NA antigenic drift.

Results

Generation of H3N2-derived NA immune sera in ferrets and mice

Our aim was to determine the antigenic relationship between NAs derived from human H3N2 viruses that circulated during nearly one decade. We first selected 43 H3N2 neuraminidase protein sequences obtained via GISAID, derived from viruses that were isolated between 2009 and 2017 (Elbe and Buckland-Merrett, 2017). Hierarchical clustering with minimax linkage was employed to ensure the set was representative of overall protein sequence diversity (Bien and Tibshirani, 2011). Next, 43 recombinant H1N2 viruses were generated that carried the internal and HA genes from PR8 virus and the NA genes of the selected H3N2 viruses. In addition, the corresponding tetrabrachion-stabilized recombinant N2 NA proteins were produced in Chinese hamster ovary (CHO) cells and purified, and are referred to as NACHOs (Catani et al., 2022). All purified NACHOs were tetrameric based on SEC-MALS analysis. The enzymatic activity of the NACHOs was determined based on the hydrolysis of the fluorogenic small molecule substrate 4-methylumbelliferyl-N-acetylneuraminic acid (MUNANA). The NACHOs were active with a specific activity ranging from 0.27 to 27.48 nmole/min/µg, indicating correct folding and assembly of the NA head domains (Table S1).

Immune sera against all 43 H3N2-derived NAs were generated in pairs of ferrets by a primary infection with the respective H1N2 reassortant viruses. This prime by infection was used to avoid the use of an adjuvant upon subsequent boost with the corresponding NACHOs. On day 28 after primary infection, all animals were boosted by intramuscular injection of homologous NACHO, except for the ferrets that had been primed by infection with A/Stockholm/15/2014 and A/Estonia/91621/2015, which were re-inoculated with the same respective H1N2 reassortant viruses. These two pairs of ferrets were not boosted with homologous NACHO because the corresponding NACHOs were not available at the time of the experiment. Blood samples were taken from the ferrets on days 14 and 42 after (primary) infection (Figure 1a). Priming by H1N2 infection resulted in seroconversion against the respective immobilized homologous NACHOs (Figure 1b). Subsequent immunization with recombinant NACHOs boosted the NACHO-specific IgG titers in day 42 serum samples. In contrast, serum samples from the ferrets that had been re-inoculated with H1N2 reassortant carrying NA derived from

108 A/Stockholm/15/2014 or A/Estonia/91621/2015, showed no further increase in titers, presumably
109 because prior exposure with the same H1N2 virus had induced a sterilizing immune response (Figure
110 1b).

111 We also generated NA immune sera in BALB/c mice. Groups of 5 mice were immunized two times,
112 with a two-week interval, by intramuscular injection with 1 µg of the respective 43 NACHOs
113 adjuvanted with AF03. Blood was collected from the immunized mice and serum prepared on day 28
114 after the prime immunization (Figure 1c). NACHO-specific IgG titers in the mouse immune sera, pooled
115 from each group, ranged from 1:8100 to 1:72900 (Figure 1d).

116 **The antigenic profile of N2 neuraminidase**

117 Next, NAI titers were determined in the ferret sera using a panel of H6N2 reassortant viruses in an
118 enzyme-linked lectin assay (ELLA), avoiding interference by anti-H1 HA antibodies. We generated 27
119 H6N2 influenza viruses with H6 HA derived from A/mallard/Sweden/2002 and NA derived from a
120 subset of the 43 H3N2 viruses, thereby retaining NA sequence diversity and year of H3N2 virus
121 isolation (Table S2).

122 The 43 NAs used as antigens and 27 NAs as source of NA, could be classified into 4 groups when
123 ordered according to the phylogenetic relatedness of their NA sequence (Figure 2). The conversion
124 rate of MUNANA into 4-methylumbelliferyl and acetylneuraminic acid by these H6N2 viruses revealed
125 a K_M that ranged from 20.7 to 144.8 µM as determined by the Michaelis-Menten equation (Figure 2 –
126 figure supplement 1a and table S2). Interestingly, the K_M differs between the distinct phylogenetic
127 groups (Figure 2 – figure supplement 1a). There was a negative correlation between the K_M values and
128 the dilution of the H6N2 viruses required to set the 70% maximal NA activity in ELLA (Figure 2 – figure
129 supplement 1b).

130 Using this panel of 27 H6N2s, we determined the NAI titers in the sera obtained from the 43 pairs of
131 ferrets 2 weeks after the boost. ELLAs were performed in duplicate for all serum samples against one
132 H6N2 target at the same time. The reciprocal NAI titers of the ferret sera paired with H6N2 viruses are
133 shown in table S3. In general, the NAI titers of the ferret sera were the highest against homologous
134 and phylogenetically closely related H6N2 viruses. In Figure 2, all the tested ferret sera are
135 represented in the rows and the 27 H6N2 viruses against which the sera were evaluated in ELLA are
136 presented in the columns. The serum samples were ordered according to the phylogenetic relatedness
137 of the N2 NA head domain amino acid sequences, showing that these cluster in 4 groups (G1-G4). The
138 ELLA-based IC_{50} NAI titers were normalized by the homologous ELISA titers and then plotted relative
139 to the maximum NAI titer obtained against the respective H6N2 target viruses. The heatmap thus

140 represents, for each H6N2 virus, the normalized ELLA IC_{50} titer expressed as log_2 of the fold-difference
141 relative to the serum with the highest IC_{50} value against that H6N2 virus (dark red squares indicate
142 high and blue squares low IC_{50} values) (Figure 2).

143 Next, these normalized NAI values were clustered against each of the H6N2s using the Unweighted
144 Pair Group Method with Arithmetic Mean (UPGMA), which is a distance-based method. This clustering
145 allowed to discern at least 4 major antigenic clusters (AC1 to -4) that are depicted at the top of the
146 heat map (Figure 2). It is interesting to note that the H6N2 viruses with NA antigens derived from
147 A/Wisconsin/16/15 and A/Alaska/251/15 do not segregate into AC2, as would be predicted based on
148 the phylogenetic relatedness, but cluster in AC1 based on the UPGMA. However, the overall
149 concordance of the antigenicity with the phylogenetic relatedness, based on the amino acid
150 sequences of the NA head domains, was confirmed by hierarchical clustering with bootstrapping and
151 k-means (Figure 2 – figure supplements 2a and 2b).

152 In addition, antigenic cartography analysis, based on the method described by Smith *et al*. (Smith et
153 al., 2004), resulted in a antigenic map of the N2 NAs that was in line with the 4 proposed antigenic
154 clusters (Figure 2 – figure supplement 3).

155 In line with this, a positive correlation was observed between the pairwise phylogenetic distances and
156 the normalized NAI IC_{50} values for each of the tested H6N2s (Figure 2 – figure supplement 4).

157 We further tested the NAI activity of ferrets' sera obtained 2 weeks after the prime infection against
158 at least one H6N2 virus from each antigenic cluster. These H6N2 viruses were selected based on their
159 antigenic relatedness as deduced from the ferret immune sera analysis (Figure 2) with 2
160 representatives from group 1 (Tex12, and Per09) and 1 each from group 2 (Kan17), group 3 (Hel823),
161 and group 4 (Ind11). The normalized data confirmed the antigenic clustering observed in sera after
162 boost (Figure 2 – figure supplement 5).

163 The NAI titers were also determined in the sera obtained from the 43 groups of NACHO-immunized
164 mice against 7 of the H6N2 viruses (Figure 2 – figure supplement 6a). These H6N2 viruses were
165 selected as described above with the addition of HK14 and Swi13 H6N2s, both belonging to antigenic
166 cluster 1. Serum NAI IC_{50} values against a given H6N2 virus were normalized against the IC_{50} of the
167 mouse serum that had the highest NAI titers against the tested H6N2 virus. UPGMA-based clustering
168 showed that the mouse NACHO immune sera displayed a similar recognition pattern as the ferret
169 immune sera that had been generated by H1N2 priming followed by a NACHO boost (Figure 2). For
170 example, HK14 H6N2 NA activity is strongly inhibited by sera from group 1, is poorly inhibited by most
171 of the sera from group 2 and is hardly inhibited by group 3 and 4 sera from both ferrets and mice.

172 Ind11 H6N2 NA activity, on the other hand, was inhibited by group 1 and 4, and hardly by group 2 and
173 3 immune sera. Overall, the normalized NAI IC_{50} values of the ferret and mouse immune sera
174 correlated very well with coefficients values ranging from 0.33 to 0.78 (Figure 2 – figure supplement
175 6b).

176 **Association analysis reveals amino acid residue substitutions that strongly impact NAI**

177 NA of human influenza viruses is subject to antigenic drift, predominantly driven by the NAI activity
178 that is detectable in the host serum (Air et al., 1985; Yasuhara et al., 2019). There are a total of 102
179 amino acid differences between the head domains of the NAs that were used to generate the 43 ferret
180 immune sera (Figure 3 - Figure supplement 1).

181 These 102 variable amino acids in the N2 head domain are predominantly exposed on the NA surface
182 (Figure 3– figure supplement 2).

183 To try to identify which of these amino acid substitutions have a significant impact on NAI, we
184 performed an association analysis for each of the tested H6N2 viruses. For this analysis, the NAI IC_{50}
185 value was compared between groups of N2 sera according to the presence or absence of a substitution
186 of any of the 102 amino acid position that are different between the panel of 43 tested N2s against
187 which sera had been raised in ferrets. As a result, a p-value is obtained for each position that reflects
188 its possible impact on NAI (Figure 3a). The significance values higher than 1.3 ($p<0.05$) of
189 representative strains of the 4 antigenic groups were represented on the surface of N2 (Figure 3b). No
190 obvious antigenic patches, however, could be distinguished on the N2 NA surface.

191 A similar association analysis was performed using the NAI values obtained with the mouse NACHO
192 immune sera. The calculated p-values obtained from the mouse and ferret NAI data were in line with
193 each other (Figure 3 – figure supplement 3).

194 **Residues close to the catalytic pocket are more likely to impact NAI**

195 We next calculated the distance between the Cα atom of each amino acid present in the N2 structure
196 (PDB: 6BR6, from A/Perth/16/2009 NA) to each Cα of the variable amino acids present in the panel.
197 We then determined the correlation of those distances with the p-values that were previously
198 determined in the association analysis. The resulting correlation coefficients (Tau values) indicate a
199 similar pattern among all 27 tested H6N2s (Figure 4a). When visualized on the N2 surface structure,
200 the Tau values revealed a geometrical distribution with the negative correlations being in closer
201 proximity to the catalytic pocket (Figure 4b). Similar data was obtained when mice sera were analyzed
202 this way (Figure 4 – figure supplement 1).

203 **Prediction of the N2 antigenicity based on a machine learning method**

204 The antigenic drift of human H3 HA has been extensively studied and modelled (Meyer and Wilke,
205 2015; Smith et al., 2004; Westgeest et al., 2012; Wu et al., 2020). To model the NA drift observed in
206 our panel of N2 NAs, we first calculated the antigenic distances between the distinct NA sera, using a
207 similar approach as has been used to visualize the HA antigenic map (Cai et al., 2012). Then, using the
208 antigenic distances and a random forest method (RF), a model was built based on amino acid sequence
209 information. A similar model has been used by Yao *et al.* to predict the antigenicity of H3 HA (Yao et
210 al., 2017). Here, the optimized model was built using a combination of 25 randomly sampled features
211 in 1500 decision trees. The resulting model generates predictive antigenic distances that strongly
212 correlate with the observed values (Figure 5a), with an RMSE/mean=0.207). The RF also enables
213 scoring of amino acid residues according to their importance in the decision trees. One measure of
214 importance can be defined as how early a change in a position is placed in the generated decision
215 trees (mean minimal depth). Another measure of importance is how much the standard error mean
216 increases when a variable is permuted. Finally, the prevalence of a variable amino acid in nodes of the
217 decision tree can also indicate its importance. Those importance scores were represented in a multi-
218 way plot (Figure 5b). The importance scores highlighted similar positions as previously determined in
219 the association study. Finally, we used NA sequences of recent seasonal influenza vaccine
220 recommended H3N2 strains to predict their antigenic distance relative to our panel of N2s, including
221 3 recent N2 NA components (from A/HongKong/45/2019, A/Tasmania/503/2020, and
222 A/Darwin/6/2021) that were not present in our data set. The predicted antigenic distances were
223 plotted in the heatmap in a red to blue scale, indicating high to low antigenic distance, respectively
224 (Figure 5c). The RF clearly reproduced the drift observed in AC2 versus AC1. The modelling also
225 indicates that the antigenic distance of the 3 recent N2s to their corresponding group 2 NAs is
226 increasing (represented by the dark blue turning light blue, from the A/Singapore/infimh-16-
227 0019/2016 towards the A/Darwin/6/2021 in G2) whereas their distance to group 4 NAs is decreasing
228 (dark red becoming yellow from the A/Singapore/infimh-16-0019/2016 towards the A/Darwin/6/2021
229 in G4).

230 **Discussion**

231 The sequence diversity of N2 proteins derived from the 43 selected human H3N2 viruses isolated
232 between 2009 and 2017 allows to classify them in 4 major phylogenetic groups. Group 1 contains 22
233 N2 NAs, 4 of which were derived from vaccine recommended H3N2 strains: A/Perth/16/2009,
234 A/Texas/50/2012, A/Switzerland/9715293/2013, and A/Hong Kong/4801/2014. Phylogenetic group 2
235 comprises 14 N2 NAs, one of which is derived from a vaccine H3N2 recommended strain:

236 A/Singapore/INFIMH-16-0019/2016. The third phylogenetic group contains two NAs that are derived
237 from H3N2 strains that had been isolated in Helsinki in 2013. Remarkably, the NA sequence of these
238 two strains is closely related to that of H3N2s that circulated more than 15 years earlier (e.g. 99%
239 identity with NA of A/Sydney/5/1997). The fourth phylogenetic group is composed of NAs derived
240 from zoonotic cases with swine H3N2 strains isolated between 2012 and 2017. Swine-to-human
241 transmission of H3N2 viruses have occurred multiple times in the USA in 2012 and continue to be
242 detected at low frequency until to date (CDC, 2023; Elbe and Buckland-Merrett, 2017).

243 We assessed the antigenic diversity of the NA panel by generating 27 recombinant H6N2 viruses and
244 43 ferret NA immune sera produced by H1N2 priming followed by boosting with homologous
245 recombinant NA (NACHO; n = 41) or by reinfection with H1N2 (A/Estonia/91621/2015 and
246 A/Stockholm/15/2014). Most of the ferrets had detectable serum anti-N2 antibodies by day 14 after
247 infection with H1N2. Anti-NA antibody titers increased after a boost with non-adjuvanted homologous
248 recombinant CHO-produced soluble tetrameric NA suggesting that the use of recombinant NA may
249 boost naturally acquired anti-NA antibody responses in the human population.

250 The NAI activity of the ferret sera against 27 tested H6N2s reassortants revealed a pattern of inhibition
251 that largely coincides with the phylogenetic distances based on the NA head domain sequences. In the
252 tested panel of H6N2s, at least 4 major antigenic groups were identified. We noted that H6N2 with
253 Kan17 NA had a broader profile of inhibition than other H6N2 viruses from group 2, being also
254 inhibited by serum raised against NA from phylogenetic groups 3 and, to a lesser extent, group 4.
255 Additionally, the H6N2s Wis15 and Ala15 have an antigenic behaviour that is more closely related to
256 antigenic cluster 1, despite belonging to group 2 according to their phylogenetic similarities. Based on
257 the NAI panel, an association analysis was performed to try to identify amino acid changes that affect
258 NAI. It is interesting to note that the amino acid substitutions S245N and S247T, combined with
259 substitution P468H, were identified in this association analysis. Those substitutions were described as
260 major contributors of the NA antigenic drift that occurred in H3N2 in 2014 (Wan et al., 2019). NAs
261 from A/Wisconsin/16/2015 and A/Alaska/251/2015 also have the S245N and S247T substitutions and
262 phylogenetically belong to group 2 NAs. However, those 2 NAs lack the P468H mutation and are
263 antigenically closer to group 1 NAs, confirming the requirement of P468H combined with the S245N
264 and S247T substitutions for this NA antigenic drift (Wan et al., 2019). This observation suggests that
265 NA antigenic drift may sometimes require a combination of amino acid changes rather than single
266 mutations. Wang and colleagues have very elegantly demonstrated that N2 antigenic evolution is
267 constrained by charge balances in an antigenic region, which can partially explain the observation that
268 NA amino acids can undergo co-evolution to result in antigenic drift (Wang et al., 2021). Interestingly,
269 NAs originated from H3N2 variants classified in phylogenetic group 4 were antigenically closer to N2s

270 belonging to phylogenetic group 1. This suggest that the antigenic drift of recent NAs from group 2
271 increases the antigenic distance from the N2s of swine origin.

272 Noteworthy, the analysis of the sera obtained from ferrets after infection shows that, despite the
273 lower homologous anti-NA titers, the inhibition pattern evaluated against 5 distinct H6N2s (composed
274 of at least one representative of each antigenic group) is in accordance with the response obtained
275 after boosting with recombinant protein. This suggests that a boost with homologous recombinant
276 soluble tetrameric NA does not alter the breadth of the antibody response induced by H1N2 infection
277 only.

278 NAI was also determined against 7 distinct H6N2 reassortant viruses using a panel of 43 anti-N2 NA
279 sera raised in mice by immunization with adjuvanted NACHOs. The observed NAI responses again
280 allowed clustering of the N2 NAs into 4 main antigenic groups, which correlates with data obtained in
281 ferrets. Studies in mice can thus offer a convenient alternative to the use of ferrets in future NA
282 antigenicity studies. This data also supports the hypothesis that there may be universal rules of
283 immunogen antigenicity and immunogenicity (Altman et al., 2015).

284 The determined K_M values of the H6N2 viruses used here, indicates that substrate affinity tends to
285 vary according to the phylogenetic relatedness of N2s. The N-glycosylation at position 245 was
286 previously described to be responsible for reducing N2 affinity for its substrate (Powell and Pekosz,
287 2020). Unlike group 2, which is primarily characterized by the presence of a N-glycan at position 245,
288 NAs from phylogenetic group 4 have a low K_M, indicating an increased affinity for substrate. This result
289 suggests that phylogenetic drift can be accompanied by changes in NA enzymatic properties.
290 Curiously, the Ala15, Wis15, and Kan17, despite having antigenic properties closer to group 1, still
291 have K_M values that are comparable to those of group 2 N2 NAs.

292 After the determination of NA antigenic distances, we used random forest modelling to estimate the
293 impact of amino acid changes on antigenic distances. We obtained a strong correlation of predicted
294 versus observed antigenic distances. However, it is important to note that the training dataset was
295 based on the 102 mutations present in our panel, limiting the predictions for other positions.
296 Furthermore, random forest enabled the classification of the variable amino acids according to
297 importance scores. Also, our modelling does not consider that substitution by other amino acids can
298 have a distinct impact on the antigenic distance. As a consequence, predictions based on the model
299 could underestimate the importance of a particular amino acid residue substitution in some cases. It
300 is important to highlight that co-occurring substitutions in our panel (the ones present in the main
301 branches of the phylogenetic tree) cannot be individually assessed by association analysis or the
302 random forest model. The individual weight of those mutation on NA drift thus remains to be

303 experimentally demonstrated. Interestingly, the modelling could put in evidence the gradual drift of
304 recent N2s which were not present in the dataset (A/Hong Kong/45/2019, A/Tasmania/503/2020, and
305 A/Darwin/6/2021).

306 It has been reported that an N-glycosylation site at position 329 combined with E344 in NA from
307 human H3N2 viruses from 2007 to 2013 was gradually lost in later H3N2 viruses (Ge et al., 2022). This
308 loss of an N-glycosylation site at position 329 combined with an E344K substitution was associated
309 with a change in NAI reactivity in ferret sera. Three N2 NAs in our panel, derived from
310 A/Victoria/361/2011, A/Hong_Kong/3089/2017, and A/Tennessee/18/2017, lack this N-glycosylation
311 motif. The E344K substitution is present in three other NAs, derived from A/Nagano/2153/2017,
312 A/Minnesota/11/2010, and A/Indiana/08/2011. The importance of those mutations is among the
313 lowest ones predicted by our modeling. However, the differences in NAI reported by Ge *et al*. are very
314 modest (less than twofold). The experimental variability in our study potentially limits the
315 identification of substitutions with a subtle impact on NAI.

316 The protective potential of NA antigen against influenza has been underscored by multiple studies. It
317 is likely that NA will be included as a standard component of next generation influenza vaccines. The
318 difficulties of producing stable tetrameric NA may be overcome in the future thanks to protein design
319 or with the advent of mRNA-based vaccines (Catani et al., 2022; Chivukula et al., 2021; Ellis et al.,
320 2022). The antigenic modelling associated with sequence surveillance may increase our predictive
321 ability, highlighting major potential drifts and support NA antigen designs that may elicit broader NAI
322 responses compared to natural NA.

323 In summary, our study shows that immunization with recombinant N2 NA immunogen can boost anti-
324 NA serum antibody responses in ferrets that were primed by infection with an influenza virus that
325 carries the homologous NA. At least 4 major antigenic groups could be distinguished in N2 NA derived
326 from human H3N2 viruses that were isolated between 2009 to 2017, and those antigenic groups
327 predominantly correspond with the phylogenetic relatedness of the N2 head domains. In addition, the
328 amino acid substitutions in close proximity of the NA catalytic pocket are more likely to affect NAI
329 patterns.

330 **Material and Methods**

331 **Rescue of H1N2 and H6N2 reassortants**

332 All reassortant H1N2 and H6N2 viruses included in the study were generated by reverse genetics, with
333 each reassortant expressing the targeted NA antigen, internal genes from A/Puerto Rico/8/1934 H1N1
334 (PR8), and the HA from PR8 H1N1 or A/mallard/Sweden/81/2002 H6N1, respectively. Briefly, HA and
335 NA segments including non-coding regions were generated by custom gene synthesis (Geneart AG),
336 while PR8 internal segments were derived from a viral isolate as previously published (Marsh and
337 Tannock, 2005). All segments were cloned into a bi-directional transcription plasmid derived from
338 pUC57 (Genscript) including polymerase (Pol) I and Pol II promoters, as previously described
339 (Hoffmann et al., 2000), and the entire set of 8 plasmids was used to transfect 293FT cells (Thermo
340 Fisher Scientific) using Lipofectamine 2000 CD (Thermo Fisher Scientific). Twenty-four hours after
341 transfection, Madin-Darby Canine Kidney Cells (MDCK-) ATL cells (ATCC) were added to the
342 transfected cells in the presence of TPCK-treated trypsin (Sigma) to allow influenza virus propagation.
343 Cell culture supernatants containing influenza virus were harvested 7 days post-MDCK addition and
344 blindly passaged in 8–10-day-old embryonated chicken eggs (Charles River Laboratories, Inc.).
345 Inoculated eggs were incubated at 37°C for 48 h, then cooled to 4°C for 12 h, prior to allantoic fluid
346 harvest and clarification by low-speed centrifugation (3,000 rpm, 20 min). For H6N2 viruses only, high-
347 yield stocks were generated by an additional passage in eggs as described above. Virus titers were
348 determined by plaque assay on MDCK cells.

349 **Design and production of recombinant proteins**

350 The coding information of the NACHO proteins was cloned under the transcriptional control of the
351 CMV promoter in the pCDNA3.4 plasmid with a CD5 secretion signal, an amino-terminal His-tag and
352 the thrombin cleavage signal followed by tetrabrachion-NA. NACHOs were expressed in a mammalian
353 cell culture system as previously described with modifications (Catani et al., 2022).

354 **Animal experiments**

355 The ferret immunization experiment was conducted at Bioqual, Inc., MD (USA). The experiments were
356 approved by the Institutional Animal Care and Use Committee of the Bioqual (reference number 17-
357 021.6). Outbred 18-22 weeks old naïve male and female Fitch ferrets were obtained from Triple F, PA
358 (USA) and housed under specified pathogen-free conditions with food and water *ad libitum*. Ferrets
359 were primed on day 0 by intranasal challenge with influenza H1N2 reassortant virus (1,000µl/dose,
360 split evenly between nostrils). Four weeks after initial infection (day 28), ferrets were immunized with
361 45 µg of NACHO (500µl/dose, intramuscularly, split evenly between hind thighs) corresponding to

362 homologous NA used in day 0 prime. Alternatively, and due to low yield of selected recombinant
363 NACHOs, ferrets were boosted on day 28 with 15 μg of homologous NACHO (A/Perth/16/2009nib-64,
364 A/Tasmania/1018/2015, A/Utah/11/2011, and A/West Virginia/17/2012) or were inoculated with the
365 same H1N2 reassortant virus used in the prime (A/Estonia/91621/2015 and A/Stockholm/15/2014).
366 Sera from bleeds two weeks after the prime (day 14) and booster vaccination (day 42) were tested for
367 immunogenicity and seroconversion in serological assays.

368 The mouse immunization experiments were conducted according to the Belgian legislation (Belgian
369 Law 14/08/1986 and Belgium Royal Decree 06/04/2010) and European legislation on protection of
370 animals used for scientific purposes (EU directives 2010/63/EU and 86/609/EEC). Experimental
371 protocols were all approved by the Ethics Committee of the Vlaams Instituut voor Biotechnologie
372 (VIB), Ghent University, Faculty of Science (EC2019-035). Female BALB/c mice, aged 6–7 weeks, were
373 purchased from Charles River. The mice were housed in a specified pathogen-free animal house with
374 food and water *ad libitum*. Animals were immunized intramuscularly in the right quadriceps.
375 Immunization was performed with 50 µl containing 1 µg of recombinant protein (tetrabrachion
376 stabilized NAs, referred to as NACHOs). All, except A/West Virginia/17/2012 NACHOs were used as
377 immunogens in mice. All immunizations were adjuvanted with a 1:1 volume of AF03 (25 µl of antigen
378 in PBS + 25 µl of AF03 per dose) (Caillet et al., 2010).

379 Two or three weeks after the boost immunization, mice were humanely sacrificed with an anaesthetic
380 overdose of Nembutal (6 mg per mouse) and bled retro-orbitally. The obtained blood samples were
381 incubated for 30 min at 37°C to allow clotting, which was followed by centrifugation at 10,500 g for 5
382 minutes. The supernatant (the serum) was recovered and submitted to a second centrifugation at
383 10,500 g for 5 minutes. Cleared sera were stored at -20°C before use in serological assays.

384 **ELISA**

385 Anti-tetNA IgG levels in mouse and ferret sera were determined by capture ELISA using tetNAs in
386 Pierce™ nickel-coated plates (cat. # 15442). Recombinant proteins were diluted in DPBS (Life
387 technologies cat. # 14040-182) (tetNA was diluted to 0.5 µg/ml). Then, 50 µl of the coating antigen
388 solutions was added to each well and the plate was incubated at room temperature for 1 h on a
389 shaking platform. The wells of the plates were then washed 3 times with PBS-T (Sigma cat. # P3563-
390 10PAK) and blocked for 1h with 1% BSA (for the mouse sera) or 10% milk (for the ferret sera) in DPBS.
391 After blocking, the wells of the plates were washed once with PBS-T and incubated with a 3-fold serial
392 dilution, starting at a 1/100 dilution, of serum in DPBS, 0.5% BSA, 0.05% tween-20 for 2h at room
393 temperature on a shaking platform. The wells of the plates were then washed 5 times with PBS-T and
394 incubated with a 1:5000 dilution of anti-mouse IgG-HRP (GE healthcare cat. # NA931-1ml), or with a

395 1:100000 dilution of anti-ferret IgG-HRP (Abcam cat. # 112770) in DPBS, 0.5% BSA, 0.05% Tween-20.
396 The 3,3',5,5'-tetramethylbenzidine (TMB) substrate (BD cat. # 555214) was added after 3 washes with
397 PBS-T and the reaction was stopped after 5 min by addition of 50 µl of 1 M H_2SO_4. The optical density
398 (O.D.) in each well was determined at 450 nm and, as a reference, 655 nm using an iMark™ Microplate
399 Absorbance Reader (Bio-rad). The end point titer was determined for each serum sample by scoring
400 the dilution that resulted in an O.D. that was equal to or 2 times higher than the background O.D.
401 obtained from pre-immune control sera dilution series.

402 **Enzyme-linked lectin assay to determine neuraminidase inhibition titers**

403 Fetuin (Sigma cat. # F3385) was diluted into coating buffer (KPL cat. # 50-84-01) to a concentration of
404 25 µg/ml and 50 µl was added to the wells of Nunc MaxiSorp™ plates (Thermofisher cat. # 44-2404-
405 21), which were incubated overnight at 4°C. The coated plates were then washed 3 times with PBS-T
406 (Sigma cat. # P3563-10PAK) and incubated overnight with 60 µl of a dilution of H6N2 and 60 µl of 2-
407 fold serial dilution of serum, starting at a 1/20 dilution, in sample buffer (1X MES VWR cat. # AAJ61979-
408 AP: 20mM $CaCl_2$, 1% BSA, 0.5% Tween-20). These dilutions of the H6Nx viruses correspond to the 70%
409 maximum activity of NA from the respective viruses as determined in the ELLA assay. Fetuin-coated
410 plates were then washed 3 times with PBS-T and incubated for 1 h with a solution of PNA-HRP (cat. #
411 L6135-1MG, Sigma) at 5 µg/ml in conjugate diluent (MES pH 6.5, 20 mM CaCl2, 1% BSA). The plates
412 were washed 3 times with PBS-T, TMB substrate was added and then the plates were incubated for 5
413 minutes before the reaction was stopped by the addition of 50 µl of 1 M H_2SO_4. The optical density
414 was measured at 450 nm and, as a reference, 655 nm in an iMark™ Microplate Absorbance Reader
415 (Bio-rad). Half maximum inhibitory concentrations (IC_{50}) values were determined by non-linear
416 regression analysis (GraphPad Prism software).

417 **NA Enzyme Kinetics Assay**

418 The enzymatic activity of NACHOs and H6N2s was determined with the fluorogenic small substrate 4-
419 methylumbelliferyl)-α-d-*N*-acetylneuraminic acid (MUNANA) as previously described (Marathe et al.,
420 2013). First H6N2 dilutions were tested to ensure that MUNANA conversion into 4-
421 methylumbelliferone (4-MU) generated fluorescence over time at a linear ratio. Ten microliters of
422 1 mM of MUNANA (Sigma cat # M8639) in 200 mM sodium acetate buffer (pH 6.5) containing 2 mM
423 $CaCl_2$ and 1% butanol was incubated with 40 µl of PBS solution containing viral dilution. Conversion to
424 4-MU was monitored every 2 min for 1 h using a BMG Fluostar OPTIMA reader (excitation at 365 nm
425 and emission determined at 450 nm). Second, using the selected dilution of virus, the assay was
426 repeated with dilutions of MUNANA ranging from 2.5 to 100 µM. A standard curve with 800 to

427 25 pmoles/well of 4-MU (Sigma cat # M1508) was used to extrapolate the molar conversion of
428 MUNANA. K_M was calculated using GraphPad Prism version 8.4.3.

429 **Antigenic cartography**

430 Antigenic cartography was performed as described by Smith et al. (Smith et al., 2004) using the R CRAN
431 package (https://CRAN.R-project.org/package=Racmacs).

432 **Association study**

433 For the association analysis, under the assumption of homogeneous genetic relatedness among the
434 selected H3N2 virus strains, a simple linear regression model for mutation-trait association analysis
435 was fitted to the data for each H6N2 separately. The significance values were calculated by comparing
436 IC_{50} values of sera that were classified into 2 groups according to the presence or absence of variation
437 in the amino acid of reference Tex12 sequence.

438 **Correlations with distances from the NA catalytic pocket**

439 Tau values were determined by correlating distances with significance values obtained from the
440 association analysis or the importance scores obtained from machine learning. A similar method was
441 described by Meyer *et al*. to define geometrical constraints of HA evolution (Meyer and Wilke, 2015).
442 Briefly, the relative distances of amino acids were calculated based on the structure of A/Perth/2009
443 (H3N2) NA (PDB: 6BR6) (Hadházi et al., 2018). The distances were calculated from each Cα to every
444 other Cα. The distances from every residue to the 98 variable residues (4 of the 102 variable amino
445 acids are localized near the end of the stalk and are not resolved in the crystal structure) residues of
446 the that are present in the panel of N2s and the 6BR6 structure were then correlated with the
447 significance values that were obtained in the association analysis, or importance scores obtained in
448 the machine learning. Correlation coefficients were visualized on the structure of N2 NA derived from
449 pandemic A/RI/5+/1957 H2N2 virus (PDB: 4H53)(Vavricka et al., 2013) using Chimera 1.14.

450 **Random Forest algorithm**

451 The Random Forest algorithm was adapted from (Yao et al., 2017). Briefly, the non-conserved
452 positions in the multiple sequence alignment of N2 head domain amino acid sequences of all tested
453 N2s were selected. The feature matrix (X) was created by assessing matches/mismatches on each non-
454 conserved position for each pair of N2 head domain amino acid sequences as:

$$X = \begin{array}{c|cccc} & X_1 & X_2 & \cdots & X_m \\ \hline V_1V_2 & 0 & 1 & \dots & 1 \\ \vdots & \vdots & \vdots & \dots & \vdots \\ V_1V_n & 1 & 0 & \dots & 1 \\ \vdots & \vdots & \vdots & \dots & \vdots \\ V_{n-1}V_n & 1 & 0 & \dots & 1 \end{array}$$

where X_i represents the non-conserved positions in the multiple sequence alignment

m is the number of non-conserved positions (102 in total)

V_i represents the N2 head domain sequence for each tested NA

n is the number of tested sera (43 in total)

0 represents a match, 1 represents a mismatch in the alignment

The response vector (Y) is composed of the antigenic distances for each pair of tested sera. These antigenic distances were determined based on NAI, similarly to the method used to determine HI based immunogenic distances that was described by Cai *et al*. In summary, the distances between sera was calculated as $\frac{1}{n}\sum_{t=1}^{n}|d[t,i]-d[i,t]|$, which represent average distances between 2 serum samples among all tested H6N2s (Cai et al., 2012). We applied the random forest function from the randomForest package in R to construct the model. We set the bootstrapping (tree) number to 1500 and the number of features to 25 for each tree. Accuracy was determined as the root-mean-square error (RMSE), calculated using the RMSE function from the yardstick package in R.

Additionally, predicted antigenic distances of the out-of-bag samples were compared to the observed distances by fitting a linear model and calculating the R^2 value. To calculate the importance of each feature (X_i), the following metrics were calculated using the measure importance function of the randomForestExplainer package in R:

- mean minimal depth: mean of the depths of the node in each tree that splits on this feature and is the closest to the root of the tree (minimal depth). The lower, the more important the feature since a low depth means that many observations are divided into groups based on this feature.
- mse decrease: mean decrease of accuracy in predictions on out of bag samples when the feature is excluded from the model. The higher, the more important the feature.
- number of nodes: total number of nodes in the forest that use the feature for splitting. The higher, the more important the feature.

The data and code used for the generation of the rf model is available at https://github.com/SaelensLAB/RF.

Acknowledgements

We gratefully acknowledge all data contributors, i.e., the Authors and their Originating laboratories responsible for obtaining the specimens, and their Submitting laboratories for generating the genetic sequence and metadata and sharing via the GISAID Initiative, on which this research is based.

We are grateful to the animal caretakers of the animal house at the VIB-UGent Center for Inflammation Research.

Competing interests

XS reports grants from Sanofi Vaccines. GCG, TS, RG, JH, JC, IVU, TF, SS, SR, LR, and TUV are or were Sanofi employees and may hold shares and/or stock options in the company.

Disclosure of funding sources

This work was funded by Sanofi Vaccines.

Author Contributions

JPPC, TY, AS, IVU, TF, RG, JH, SS, SR, LL and JC performed experimental work. JPPC, TY, AS, RG, GCG, TUV, and XS designed the experiments, analyzed and interpreted the data. JM and MV analyzed the data. JPPC and XS wrote the manuscript and are accountable for accuracy and integrity of the work. All authors proofread and critically reviewed the manuscript.

501 **References**

502 Air GM, Els MC, Brown LE, Laver WG, Webster RG. 1985. Location of antigenic sites on the three-
503 dimensional structure of the influenza N2 virus neuraminidase. *Virology* **145**:237–248.
504 doi:10.1016/0042-6822(85)90157-6
505 Altman MO, Bennink JR, Yewdell JW, Herrin BR. 2015. Lamprey VLRB response to influenza virus
506 supports universal rules of immunogenicity and antigenicity. *eLife* **4**:e07467.
507 doi:10.7554/eLife.07467
508 Bedford T, Suchard MA, Lemey P, Dudas G, Gregory V, Hay AJ, McCauley JW, Russell CA, Smith DJ,
509 Rambaut A. 2014. Integrating influenza antigenic dynamics with molecular evolution. *eLife*
510 **3**:e01914. doi:10.7554/eLife.01914
511 Belongia EA, Simpson MD, King JP, Sundaram ME, Kelley NS, Osterholm MT, McLean HQ. 2016.
512 Variable influenza vaccine effectiveness by subtype: a systematic review and meta-analysis
513 of test-negative design studies. *The Lancet Infectious Diseases* **16**:942–951.
514 doi:10.1016/S1473-3099(16)00129-8
515 Bien J, Tibshirani R. 2011. Hierarchical Clustering With Prototypes via Minimax Linkage. *J Am Stat*
516 *Assoc* **106**:1075–1084.
517 Cai Z, Zhang T, Wan X-F. 2012. Antigenic Distance Measurements for Seasonal Influenza Vaccine
518 Selection. *Vaccine* **30**:448–453. doi:10.1016/j.vaccine.2011.10.051
519 Caillet C, Piras F, Bernard M-C, de Montfort A, Boudet F, Vogel FR, Hoffenbach A, Moste C, Kusters I.
520 2010. AF03-adjuvanted and non-adjuvanted pandemic influenza A (H1N1) 2009 vaccines
521 induce strong antibody responses in seasonal influenza vaccine-primed and unprimed mice.
522 *Vaccine* **28**:3076–3079. doi:10.1016/j.vaccine.2010.02.050
523 Catani JPP, Job ER, Ysenbaert T, Smet A, Ray S, LaRue L, Stegalkina S, Barro M, Vogel TU, Saelens X.
524 2022. Pre-existing antibodies directed against a tetramerizing domain enhance the immune
525 response against artificially stabilized soluble tetrameric influenza neuraminidase. *npj*
526 *Vaccines* **7**:1–9. doi:10.1038/s41541-022-00435-7
527 CDC. 2023. Novel Influenza A Virus Infections. *Fluview*.
528 https://gis.cdc.gov/grasp/fluview/Novel_Influenza.html
529 Chen YQ, Wohlbold TJ, Zheng NY, Huang M, Huang Y, Neu KE, Lee J, Wan H, Rojas KT, Kirkpatrick E,
530 Henry C, Palm AKE, Stamper CT, Lan LYL, Topham DJ, Treanor J, Wrammert J, Ahmed R,
531 Eichelberger MC, Georgiou G, Krammer F, Wilson PC. 2018. Influenza Infection in Humans
532 Induces Broadly Cross-Reactive and Protective Neuraminidase-Reactive Antibodies. *Cell*
533 **173**:417-429.e10. doi:10.1016/j.cell.2018.03.030
534 Chivukula S, Plitnik T, Tibbitts T, Karve S, Dias A, Zhang D, Goldman R, Gopani H, Khanmohammed A,
535 Sarode A, Cooper D, Yoon H, Kim Y, Yan Y, Mundle ST, Groppo R, Beauvais A, Zhang J,
536 Anosova NG, Lai C, Li L, Ulinski G, Piepenhagen P, DiNapoli J, Kalnin KV, Landolfi V,
537 Swearingen R, Fu T-M, DeRosa F, Casimiro D. 2021. Development of multivalent mRNA
538 vaccine candidates for seasonal or pandemic influenza. *NPJ Vaccines* **6**:153.
539 doi:10.1038/s41541-021-00420-6
540 Couch RB, Atmar RL, Franco LM, Quarles JM, Wells J, Arden N, Niño D, Belmont JW. 2013. Antibody
541 Correlates and Predictors of Immunity to Naturally Occurring Influenza in Humans and the
542 Importance of Antibody to the Neuraminidase. *The Journal of Infectious Diseases* **207**:974–
543 981. doi:10.1093/infdis/jis935
544 Cox RJ. 2013. Correlates of protection to influenza virus, where do we go from here? *Hum Vaccin*
545 *Immunother* **9**:405–408. doi:10.4161/hv.22908
546 de Vries E, Du W, Guo H, de Haan CAM. 2020. Influenza A Virus Hemagglutinin–Neuraminidase–
547 Receptor Balance: Preserving Virus Motility. *Trends in Microbiology* **28**:57–67.
548 doi:10.1016/j.tim.2019.08.010
549 Deroo T, Min Jou W, Fiers W. 1996. Recombinant neuraminidase vaccine protects against lethal
550 influenza. *Vaccine* **14**:561–569. doi:10.1016/0264-410X(95)00157-V

551 Eickhoff TC, Meiklejohn G. 1969. Protection against Hong Kong influneza by adjuvant vaccine
552 containing A2-Ann Arbor-67. *Bull World Health Organ* **41**:562–563.
553 Elbe S, Buckland-Merrett G. 2017. Data, disease and diplomacy: GISAID's innovative contribution to
554 global health. *Global Challenges* **1**:33–46. doi:10.1002/gch2.1018
555 Ellis D, Lederhofer J, Acton OJ, Tsybovsky Y, Kephart S, Yap C, Gillespie RA, Creanga A, Olshefsky A,
556 Stephens T, Pettie D, Murphy M, Sydeman C, Ahlrichs M, Chan S, Borst AJ, Park Y-J, Lee KK,
557 Graham BS, Veesler D, King NP, Kanekiyo M. 2022. Structure-based design of stabilized
558 recombinant influenza neuraminidase tetramers. *Nat Commun* **13**:1825.
559 doi:10.1038/s41467-022-29416-z
560 Ge J, Lin X, Guo Jinlei, Liu Ling, Li Z, Lan Y, Liu Liqi, Guo Junfeng, Lu J, Huang W, Xin L, Wang D, Qin K,
561 Xu C, Zhou J. 2022. The Antibody Response Against Neuraminidase in Human Influenza A
562 (H3N2) Virus Infections During 2018/2019 Flu Season: Focusing on the Epitopes of 329-N-
563 Glycosylation and E344 in N2. *Front Microbiol* **13**:845088. doi:10.3389/fmicb.2022.845088
564 Hadházi Á, Li L, Bailly B, Maggioni A, Martin G, Dirr L, Dyason JC, Thomson RJ, Gao GF, Borbás A, Ve T,
565 Pascolutti M, von Itzstein M. 2018. A Sulfonozanamivir Analogue Has Potent Anti-influenza
566 Virus Activity. *ChemMedChem* **13**:785–789. doi:10.1002/cmdc.201800092
567 Hoffmann E, Neumann G, Kawaoka Y, Hobom G, Webster RG. 2000. A DNA transfection system for
568 generation of influenza A virus from eight plasmids. *Proc Natl Acad Sci U S A* **97**:6108–6113.
569 doi:10.1073/pnas.100133697
570 Jester BJ, Uyeki TM, Jernigan DB. 2020. Fifty Years of Influenza A(H3N2) Following the Pandemic of
571 1968. *Am J Public Health* **110**:669–676. doi:10.2105/AJPH.2019.305557
572 Krammer F, Fouchier RAM, Eichelberger MC, Webby RJ, Shaw-Saliba K, Wan H, Wilson PC, Compans
573 RW, Skountzou I, Monto AS. 2018. NAction! How Can Neuraminidase-Based Immunity
574 Contribute to Better Influenza Virus Vaccines? *mBio* **9**:e02332-17. doi:10.1128/mBio.02332-
575 17
576 Leneva IA, Roberts N, Govorkova EA, Goloubeva OG, Webster RG. 2000. The neuraminidase inhibitor
577 GS4104 (oseltamivir phosphate) is efficacious against A/Hong Kong/156/97 (H5N1) and
578 A/Hong Kong/1074/99 (H9N2) influenza viruses. *Antiviral Res* **48**:101–115.
579 doi:10.1016/s0166-3542(00)00123-6
580 Maier HE, Nachbagauer R, Kuan G, Ng S, Lopez R, Sanchez N, Stadlbauer D, Gresh L, Schiller A,
581 Rajabhathor A, Ojeda S, Guglia AF, Amanat F, Balmaseda A, Krammer F, Gordon A. 2019. Pre-
582 existing anti-neuraminidase antibodies are associated with shortened duration of influenza
583 A (H1N1)pdm virus shedding and illness in naturally infected adults. *Clinical Infectious*
584 *Diseases*. doi:10.1093/cid/ciz639
585 Marathe BM, Lévêque V, Klumpp K, Webster RG, Govorkova EA. 2013. Determination of
586 Neuraminidase Kinetic Constants Using Whole Influenza Virus Preparations and Correction
587 for Spectroscopic Interference by a Fluorogenic Substrate. *PLOS ONE* **8**:e71401.
588 doi:10.1371/journal.pone.0071401
589 Marsh G, Tannock G. 2005. The role of reverse genetics in the development of vaccines against
590 respiratory viruses. *Expert Opin Biol Ther* **5**:369–380. doi:10.1517/14712598.5.3.369
591 Matrosovich MN, Matrosovich TY, Gray T, Roberts NA, Klenk H-D. 2004. Neuraminidase Is Important
592 for the Initiation of Influenza Virus Infection in Human Airway Epithelium. *Journal of Virology*
593 **78**:12665–12667. doi:10.1128/jvi.78.22.12665-12667.2004
594 Memoli MJ, Shaw PA, Han A, Czajkowski L, Reed S, Athota R, Bristol T, Fargis S, Risos K, Powers JH,
595 Davey RT, Taubenberger JK. 2016. Evaluation of Antihemagglutinin and Antineuraminidase
596 Antibodies as Correlates of Protection in an Influenza A/H1N1 Virus Healthy Human
597 Challenge Model. *mBio* **7**:e00417-16. doi:10.1128/mBio.00417-16
598 Meyer AG, Wilke CO. 2015. Geometric Constraints Dominate the Antigenic Evolution of Influenza
599 H3N2 Hemagglutinin. *PLOS Pathogens* **11**:e1004940. doi:10.1371/journal.ppat.1004940

Monto ArnoldS, Kendal AlanP. 1973. EFFECT OF NEURAMINIDASE ANTIBODY ON HONG KONG INFLUENZA. *The Lancet*, Originally published as Volume 1, Issue 7804 **301**:623–625. doi:10.1016/S0140-6736(73)92196-X

Monto AS, Petrie JG, Cross RT, Johnson E, Liu M, Zhong W, Levine M, Katz JM, Ohmit SE. 2015. Antibody to influenza virus neuraminidase: An independent correlate of protection. *Journal of Infectious Diseases* **212**:1191–1199. doi:10.1093/infdis/jiv195

Nachbagauer R, Choi A, Hirsh A, Margine I, Iida S, Barrera A, Ferres M, Albrecht RA, García-Sastre A, Bouvier NM, Ito K, Medina RA, Palese P, Krammer F. 2017. Defining the antibody cross-reactome directed against the influenza virus surface glycoproteins. *Nat Immunol* **18**:464–473. doi:10.1038/ni.3684

Ng S, Nachbagauer R, Balmaseda A, Stadlbauer D, Ojeda S, Patel M, Rajabhathor A, Lopez R, Guglia AF, Sanchez N, Amanat F, Gresh L, Kuan G, Krammer F, Gordon A. 2019. Novel correlates of protection against pandemic H1N1 influenza A virus infection. *Nature Medicine* **25**:962–967. doi:10.1038/s41591-019-0463-x

Palese P, Tobita K, Ueda M, Compans RW. 1974. Characterization of temperature sensitive influenza virus mutants defective in neuraminidase. *Virology* **61**:397–410. doi:10.1016/0042-6822(74)90276-1

Potter BI, Kondor R, Hadfield J, Huddleston J, Barnes J, Rowe T, Guo L, Xu X, Neher RA, Bedford T, Wentworth DE. 2019. Evolution and rapid spread of a reassortant A(H3N2) virus that predominated the 2017–2018 influenza season. *Virus Evol* **5**:vez046. doi:10.1093/ve/vez046

Powell H, Pekosz A. 2020. Neuraminidase antigenic drift of H3N2 clade 3c.2a viruses alters virus replication, enzymatic activity and inhibitory antibody binding. *PLOS Pathogens* **16**:e1008411. doi:10.1371/journal.ppat.1008411

Rajendran M, Nachbagauer R, Ermler ME, Bunduc P, Amanat F, Izikson R, Cox M, Palese P, Eichelberger M, Krammer F. 2017. Analysis of anti-influenza virus neuraminidase antibodies in children, adults, and the elderly by ELISA and enzyme inhibition: Evidence for original antigenic sin. *mBio* **8**. doi:10.1128/mBio.02281-16

Rosu ME, Kok A, Bestebroer TM, de Meulder D, Verveer EP, Pronk MR, Dekker LJM, Luider TM, Richard M, van den Brand JMA, Fouchier RAM, Herfst S. 2022. Contribution of Neuraminidase to the Efficacy of Seasonal Split Influenza Vaccines in the Ferret Model. *J Virol* **96**:e0195921. doi:10.1128/jvi.01959-21

Smith DJ, Lapedes AS, de Jong JC, Bestebroer TM, Rimmelzwaan GF, Osterhaus ADME, Fouchier RAM. 2004. Mapping the antigenic and genetic evolution of influenza virus. *Science* **305**:371–376. doi:10.1126/science.1097211

Uyeki TM, Hui DS, Zambon M, Wentworth DE, Monto AS. 2022. Influenza. *The Lancet* **400**:693–706. doi:10.1016/S0140-6736(22)00982-5

Vavricka CJ, Liu Y, Kiyota H, Sriwilaijaroen N, Qi J, Tanaka K, Wu Y, Li Q, Li Y, Yan J, Suzuki Y, Gao GF. 2013. Influenza neuraminidase operates via a nucleophilic mechanism and can be targeted by covalent inhibitors. *Nature Communications* **4**. doi:10.1038/ncomms2487

Viboud C, Grais RF, Lafont BAP, Miller MA, Simonsen L. 2005. Multinational Impact of the 1968 Hong Kong Influenza Pandemic: Evidence for a Smoldering Pandemic. *The Journal of Infectious Diseases* **192**:233–248. doi:10.1086/431150

Wan H, Gao J, Yang H, Yang S, Harvey R, Chen YQ, Zheng NY, Chang J, Carney PJ, Li X, Plant E, Jiang L, Couzens L, Wang C, Strohmeier S, Wu WW, Shen RF, Krammer F, Cipollo JF, Wilson PC, Stevens J, Wan XF, Eichelberger MC, Ye Z. 2019. The neuraminidase of A(H3N2) influenza viruses circulating since 2016 is antigenically distinct from the A/Hong Kong/4801/2014 vaccine strain. *Nature Microbiology* **4**:2216–2225. doi:10.1038/s41564-019-0522-6

Wan H, Qi L, Gao J, Couzens LK, Jiang L, Gao Y, Sheng Z-M, Fong S, Hahn M, Khurana S, Taubenberger JK, Eichelberger MC. 2018. Comparison of the Efficacy of N9 Neuraminidase-Specific Monoclonal Antibodies against Influenza A(H7N9) Virus Infection. *Journal of Virology* **92**:e01588-17. doi:10.1128/JVI.01588-17

651 Wang Y, Lei R, Nourmohammad A, Wu NC. 2021. Antigenic evolution of human influenza H3N2
652 neuraminidase is constrained by charge balancing. *eLife* **10**:e72516. doi:10.7554/eLife.72516
653 Weiss CD, Wang W, Lu Y, Billings M, Eick-Cost A, Couzens L, Sanchez JL, Hawksworth AW, Seguin P,
654 Myers CA, Forshee R, Eichelberger MC, Cooper MJ. 2019. Neutralizing and Neuraminidase
655 Antibodies Correlate With Protection Against Influenza During a Late Season A/H3N2
656 Outbreak Among Unvaccinated Military Recruits. *Clinical Infectious Diseases* 1–7.
657 doi:10.1093/cid/ciz1198
658 Westgeest KB, de Graaf M, Fourment M, Bestebroer TM, van Beek R, Spronken MIJ, de Jong JC,
659 Rimmelzwaan GF, Russell CA, Osterhaus ADME, Smith GJD, Smith DJ, Fouchier RAM. 2012.
660 Genetic evolution of the neuraminidase of influenza A (H3N2) viruses from 1968 to 2009 and
661 its correspondence to haemagglutinin evolution. *J Gen Virol* **93**:1996–2007.
662 doi:10.1099/vir.0.043059-0
663 Wohlbold TJ, Podolsky KA, Chromikova V, Kirkpatrick E, Falconieri V, Meade P, Amanat F, Tan J,
664 Tenoever BR, Tan GS, Subramaniam S, Palese P, Krammer F. 2017. Broadly protective murine
665 monoclonal antibodies against influenza B virus target highly conserved neuraminidase
666 epitopes. *Nature Microbiology* **2**:1415–1424. doi:10.1038/s41564-017-0011-8
667 Wu NC, Otwinowski J, Thompson AJ, Nycholat CM, Nourmohammad A, Wilson IA. 2020. Major
668 antigenic site B of human influenza H3N2 viruses has an evolving local fitness landscape. *Nat*
669 *Commun* **11**:1233. doi:10.1038/s41467-020-15102-5
670 Yao Y, Li X, Liao B, Huang L, He P, Wang F, Yang Jiasheng, Sun H, Zhao Y, Yang Jialiang. 2017.
671 Predicting influenza antigenicity from Hemagglutintin sequence data based on a joint
672 random forest method. *Sci Rep* **7**:1545. doi:10.1038/s41598-017-01699-z
673 Yasuhara A, Yamayoshi S, Kiso M, Sakai-Tagawa Y, Koga M, Adachi E, Kikuchi T, Wang IH, Yamada S,
674 Kawaoka Y. 2019. Antigenic drift originating from changes to the lateral surface of the
675 neuraminidase head of influenza A virus. *Nature Microbiology* **4**:1024–1034.
676 doi:10.1038/s41564-019-0401-1
677 Yen H-L, Herlocher LM, Hoffmann E, Matrosovich MN, Monto AS, Webster RG, Govorkova EA. 2005.
678 Neuraminidase Inhibitor-Resistant Influenza Viruses May Differ Substantially in Fitness and
679 Transmissibility. *Antimicrob Agents Chemother* **49**:4075–4084. doi:10.1128/AAC.49.10.4075-
680 4084.2005
681

682

683 **Table S1. Specific activity of the recombinant NACHOs.**

H3N2 strain NA source	Specific Activity nmole/min.µg
A/Stockholm/32/2014	9,62
A/Switzerland/9715293/2013	6,52
A/Hong Kong/4801/2014	4,13
A/Paris/2379/2014	2,42
A/Texas/50/2012	5,21
A/Stockholm/14/2012	2,42
A/Tehran/996/2012	8,46
A/Victoria/361/2011	2,71
A/Newcastle/67/2016	3,22
A/Estonia/91621/2015	5,3
A/Ankara/2396/2015	2,62
A/Stockholm/15/2014	1,14
A/Dakar/14/2014	2,37
A/PortoAlegre/Lacenrs-2376/2014	2,55
A/Utah/11/2011	1,40
A/Hokkaido/IOH079/2011	0,84
A/Gambia/G0071436/2012	1,60
A/Hanoi/Eli15597/2015	3,29
A/XinJiang-Tianshan/1411/2012	0,27
A/Perth/16/2009nib-64	5,3
A/Tasmania/1018/2015	27,48
A/NewCaledonia/23/2016	8,55
A/Alaska/251/2015	4,29
A/Hatay/4990/2016	5,83
A/Tennessee/18/2017	5,99
A/Singapore/Infimh160019/2016	8,01
A/Brisbane/273/2016	6,94
A/Poland/19b/2017	5,81
A/Wisconsin/16/2015	1,40
A/Indiana/08/2011	4,13
A/Hong-Kong/3089/2017	6,17
A/Nagano/2153/2017	2,29
A/Sweden/3/2017	2,76
A/Catalonia/9503s/2017	1,31
A/Moramanga/1907/2017	2,09
A/Heilongjiang_Xiangyan/1134/2011	6,61
A/Helsinki/823/2013	6,53
A/Helsinki/941/2013	7,02
A/Ohio/13/2017	2,59

A/Ohio/62/2012	4,28
A/Ontario/RV3236/2016	3,89
A/Indiana/18/2017	4,27
A/Minnesota/11/2010	4,25

686 **Table S2. H6N2 reassortant viruses used in the ELLA assay.**

H6Nx reassortant(*)	Titer (PFU/ml)	dilution to 70% max activity (ELLA)	K_M (MUNANA)
A/Ohio/62/2012 (Ohi12)	2.00E+08	2269.7	20.7
A/Indiana/08/2011 (Ind11)	2.50E+08	750.9	40.1
A/Ohio/13/2017 (Ohi17)	3.00E+08	521.5	33.5
A/Ontario/Rv3236/2016 (Ont16)	1.75E+08	504.1	31.5
A/Minnesota/11/2010 (Min10)	2.00E+08	1031.4	41.3
A/Helsinki/823/2013 (Hel823)	1.50E+08	155.2	45.9
A/Helsinki/941/2013 (Hel941)	3.50E+08	341.6	45.3
A/Nagano/2153/2017 (Nag17)	2.50E+08	213.6	97.8
A/Singapore/Infimh-16-0019/2016 (Sin16)	6.50E+07	257.1	93.3
A/Hong_Kong/3089/2017 (HK17)	2.00E+08	301.6	85.2
A/Sweden/3/2017 (Swe17)	6.00E+08	97	71.5
A/Moramanga/1907/2017 (Mor17)	1.40E+08	151.4	56.8
A/Kansas/14/2017 (Kan17)	2.50E+08	249	108.7
A/Wisconsin/16/2015 (Wis15)	2.00E+08	63.3	79.6
A/Gambia/G0071436/2012 (Gam12)	2.50E+08	331.5	63.6
A/Heilongjiang-Xiangyang/1134/2011 (Hei11)	2.10E+08	195.6	31.1
A/Perth/16/2009 (Per09)	3.20E+08	630.8	56.4
A/Newcastle/67/2016 (NCas16)	1.50E+08	150.4	48.5
A/Tasmania/1018/2015 (Tas15)	1.70E+08	139.5	54.8
A/Hanoi/Eli15597/2015 (Han15)	1.40E+08	94.6	82.2
A/Alaska/251/2015 (Ala15)	4.50E+08	93.7	144.8
A/Estonia/91621/2015 (Est15)	2.00E+08	281.9	62.1
A/Victoria/361/2011 (Vic11)	3.00E+08	570.3	51.1
A/Utah/11/2011 (Uta11)	2.50E+08	356.3	51.9
A/Switzerland/9715293/2013 (Swi13)	2.70E+08	160.8	64
A/Hong Kong/4801/2014 (HK14)	4.00E+07	106.3	54.7
A/Texas/50/2012 (Tex12)	2.00E+08	276.6	45.1

687 *Name of the virus from which the N2 NA in H6N2 reassortant virus was derived. The short name as used in the
688 manuscript text is mentioned between brackets.

689

690

691 **Table S3 . NAI titers against H6N2 viruses of ferret sera obtained after the boost (Part I of II).**

Sera	Swi13	HK14	Tex12	Vic11	Ncas16	Est15	Uta11	Gam12	Han15	Hei11	Per09	Tas15	Ala15
A/Switzerland/9715293/2013	**9333.0**	6833.5	10301.6	2442.3	1489.8	5530.4	1460.6	3489.9	5253.8	1510.9	1899.6	1649.9	1812.3
A/Hong_Kong/4801/2014	7527.5	**10566.4**	14983.0	2559.1	4579.4	7944.5	3590.3	7065.0	4798.3	1971.2	2522.9	3842.2	4980.9
A/Texas/50/2012	10751.3	10397.6	**8843.5**	2089.6	740.9	3821.0	902.1	1519.1	1453.1	1112.9	2506.5	835.8	1490.8
A/Victoria/361/2011(Ivr-165)	16804.7	11568.3	11892.0	**3863.7**	1868.9	3480.4	2250.0	670.9	3963.3	1379.1	2888.7	883.1	1531.9
A/Newcastle/67/2016	7647.2	9702.6	5244.0	1056.9	**4218.8**	2295.9	5477.0	821.2	1515.9	1254.3	1304.0	1253.1	1021.6
A/Estonia/91621/2015	1277.1	1379.5	911.1	387.1	290.5	**2832.9**	277.9	335.3	225.6	272.5	193.3	217.2	70.9
A/Utah/11/2011	6121.8	6591.4	6253.2	3392.5	1570.0	3727.5	**2893.7**	1294.7	2496.3	4050.7	2196.7	376.0	869.2
A/Gambia/G0071436/2012	5513.7	6192.0	5040.0	1226.5	1492.3	6342.9	772.9	**730.2**	863.5	1810.2	1399.4	836.9	888.0
A/Hanoi/Eli15597/2015	4635.2	8150.5	6232.1	872.7	1617.0	7192.3	1023.4	1343.3	**1822.0**	1969.9	1168.3	1307.0	2383.4
A/Heilongjiang-Xiangyang/1134/2011	3506.3	3480.2	5123.0	3514.3	356.0	976.7	1657.1	245.9	557.9	**7094.8**	2056.7	168.3	658.3
A/Perth/16/2009nib-64	4961.8	13872.0	8102.7	2771.2	630.3	3502.5	2644.5	1079.5	441.6	1663.8	**2458.4**	418.4	748.3
A/Tasmania/1018/2015	6503.6	7894.2	5204.6	1298.1	2335.3	2927.7	1349.1	6451.6	2374.2	709.1	2659.2	**1150.5**	977.3
A/Alaska/251/2015	7291.7	8216.5	7274.8	1247.6	1050.4	7445.9	1975.1	348.6	1070.2	1828.5	1142.7	2300.4	**3418.1**
A/Singapore/Infimh-16-0019/2016	2564.5	3869.9	3206.3	1119.2	1038.5	732.7	545.2	252.3	1308.7	196.5	328.1	399.6	778.4
A/Wisconsin/16/2015	6157.8	6249.7	3088.6	693.4	998.2	1259.1	383.6	73.1	595.7	362.7	415.4	442.8	723.5
A/Hong_Kong/3089/2017	713.6	1372.5	1290.5	391.8	312.4	670.9	231.0	144.6	161.5	143.3	88.2	317.5	702.9
A/Nagano/2153/2017	784.6	798.8	567.6	102.6	215.5	530.1	158.5	97.5	182.8	145.2	108.7	172.4	332.8
A/Sweden/3/2017	2250.6	1249.6	2688.6	1818.4	785.2	443.3	632.2	726.1	3344.3	553.2	512.0	910.7	2153.6
A/Moramanga/1907/2017	1126.6	1371.0	720.8	205.3	185.9	1073.8	339.2	212.5	335.6	228.0	201.0	396.1	603.7
A/Helsinki/823/2013	1130.4	1408.4	1382.9	491.8	77.1	1930.9	324.0	141.1	133.6	431.4	289.4	90.0	106.9
A/Helsinki/941/2013	391.1	379.7	662.2	345.4	19.2	837.0	227.2	32.7	25.7	72.6	111.1	23.7	58.9
A/Ohio/13/2017	396.6	554.6	500.2	247.4	56.6	377.9	185.1	112.0	75.2	168.4	219.8	80.1	<20
A/Ohio/62/2012	445.7	644.5	694.0	157.0	33.1	1024.6	207.9	37.9	77.9	98.5	152.6	86.9	22.5
A/Ontario/Rv3236/2016	54.0	99.2	101.7	218.0	<20	51.7	43.8	<20	<20	<20	36.9	41.1	<20
A/Indiana/08/2011	34.4	72.5	110.4	177.3	22.4	43.1	46.8	31.4	<20	40.6	36.4	<20	<20
A/Minnesota/11/2010	59.4	146.7	91.6	<20	<20	44.0	39.0	<20	<20	41.1	30.8	<20	<20

692

693 **Table S3. NAI titers against H6N2 viruses of ferret sera obtained after the boost (Part II of II).**

Sera	Sin16	Wis15	HK17	Nag17	Swe17	Mor17	Hel823	Hel941	Ohi17	Ohi12	Ont16	Ind11	Min11
A/Switzerland/9715293/2013	1291.6	939.6	1097.8	210.5	514.9	460.1	160.2	706.4	422.8	1072.5	354.5	227.5	302.5
A/Hong_Kong/4801/2014	636.5	780.7	1312.1	30.8	178.6	231.7	55.5	229.9	221.4	143.0	122.2	93.4	307.2
A/Texas/50/2012	436.8	556.3	462.7	<20	242.5	288.5	53.2	656.4	73.0	295.0	482.4	<20	149.6
A/Victoria/361/2011(Ivr-165)	568.2	1881.1	1227.3	108.5	293.8	407.7	79.3	1203.0	290.1	561.0	793.8	125.4	393.1
A/Newcastle/67/2016	192.6	246.4	411.3	18.3	70.8	125.6	206.8	259.5	893.7	1553.0	1089.8	<20	1619.5
A/Estonia/91621/2015	133.6	137.5	252.2	<20	78.5	<20	112.6	76.3	96.2	268.4	110.6	38.7	83.6
A/Utah/11/2011	212.4	753.0	215.9	41.4	138.5	265.5	100.4	549.1	208.9	1246.7	922.8	240.0	466.7
A/Gambia/G0071436/2012	390.8	532.3	694.8	37.3	174.6	139.2	296.9	470.4	233.7	154.4	423.5	157.8	709.3
A/Hanoi/Eli15597/2015	225.9	629.8	592.7	152.6	318.2	174.4	216.5	209.5	615.2	207.1	556.5	1205.8	669.2
A/Heilongjiang-Xiangyang/1134/2011	79.9	257.3	65.1	<20	77.1	34.9	475.2	76.0	236.7	1330.2	70.6	48.1	127.2
A/Perth/16/2009nib-64	263.1	535.5	249.8	<20	102.5	103.7	552.5	519.6	250.2	418.2	81.2	113.6	161.1
A/Tasmania/1018/2015	714.6	342.3	1149.8	178.8	321.5	551.2	363.1	1440.4	407.4	2702.2	819.1	463.8	689.9
A/Alaska/251/2015	655.6	1029.8	579.3	451.3	764.5	396.5	111.7	468.9	<20	72.8	88.1	<20	22.4
A/Singapore/Infimh-16-0019/2016	**3746.2**	1772.7	7210.9	1390.6	1637.5	1258.2	151.7	2123.3	94.6	282.6	68.0	<20	122.3
A/Wisconsin/16/2015	772.0	**5850.3**	678.1	373.4	680.7	420.1	<20	134.2	<20	74.7	<20	<20	<20
A/Hong_Kong/3089/2017	1534.5	708.7	**4119.2**	762.8	2114.3	744.7	297.3	324.9	<20	<20	<20	<20	<20
A/Nagano/2153/2017	501.4	157.0	1131.7	**960.8**	258.6	313.2	94.3	115.9	85.6	136.8	<20	<20	54.6
A/Sweden/3/2017	5336.2	1167.5	7099.8	1132.6	**8452.0**	4595.1	506.4	2310.2	133.0	199.5	323.9	27.2	58.5
A/Moramanga/1907/2017	1060.6	273.0	3033.6	258.9	1286.0	**6330.8**	75.6	143.2	57.3	106.0	96.7	<20	70.4
A/Helsinki/823/2013	519.3	215.9	745.1	<20	326.8	113.1	**5933.4**	11949.0	33.1	87.9	85.5	32.4	46.8
A/Helsinki/941/2013	257.3	79.5	156.3	<20	153.0	<20	3729.4	**17816.2**	<20	64.1	<20	<20	<20
A/Ohio/13/2017	28.9	<20	<20	<20	<20	<20	221.2	137.9	**2567.9**	28683.0	4819.3	781.1	4943.5
A/Ohio/62/2012	<20	<20	<20	<20	<20	<20	77.1	70.1	5592.0	**3811.0**	397.1	281.1	921.4
A/Ontario/Rv3236/2016	<20	<20	<20	<20	<20	<20	22.4	21.3	194.8	1500.5	**6167.6**	159.3	846.2
A/Indiana/08/2011	<20	<20	<20	<20	<20	<20	<20	<20	146.4	3741.8	486.8	**2910.9**	2498.3
A/Minnesota/11/2010	<20	<20	<20	<20	<20	<20	55.0	<20	202.3	509.1	726.6	380.2	**4375.6**

694

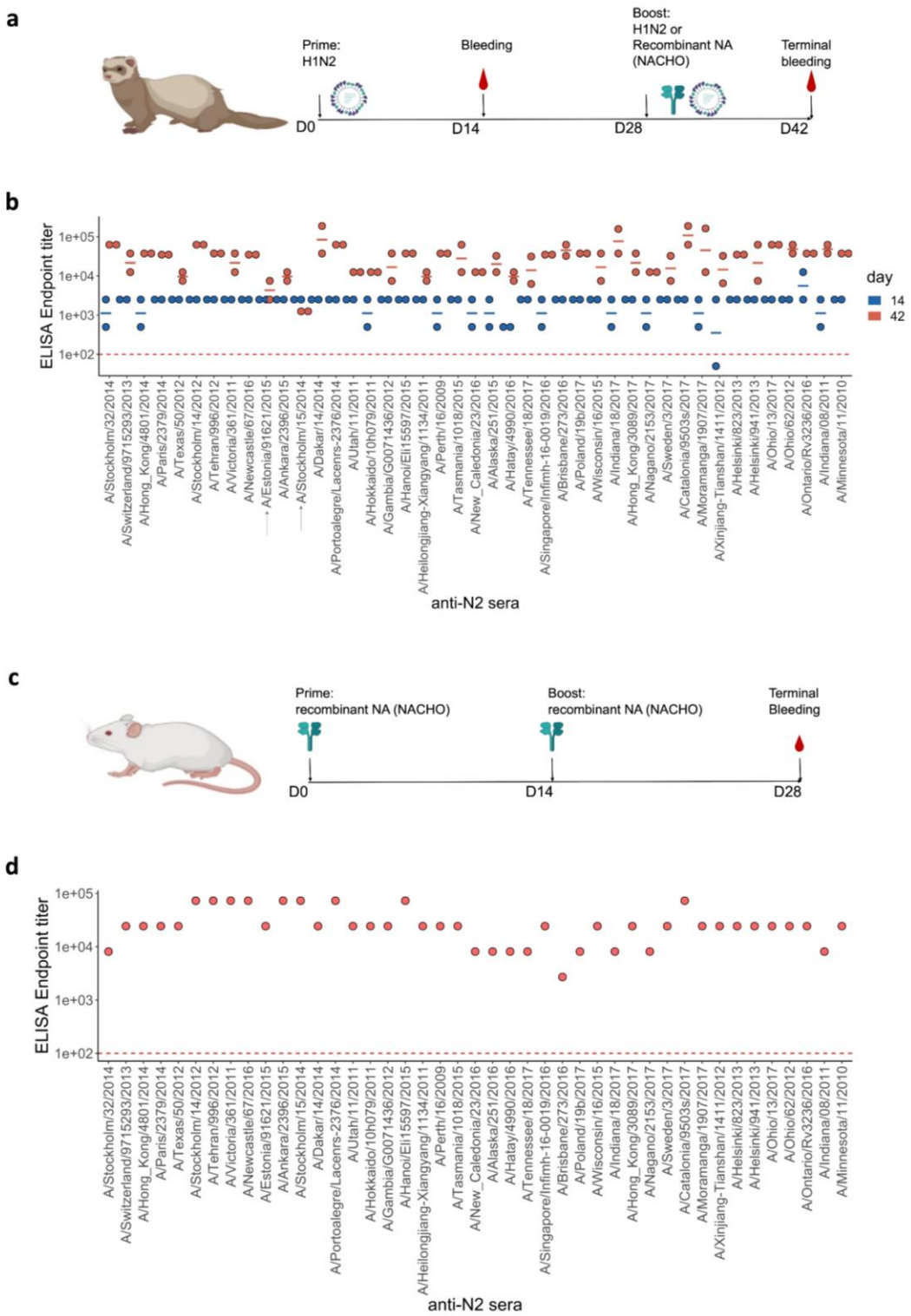

Figure 1. Generation of anti-N2 sera panel from ferrets and mice. (a) 43 Ferret immunization and blood sampling scheme. The second immunization on day 28 was performed with homologous NACHO except for the ferrets that had been primed with H1N2$_{A/Estonia/91621/2015}$ or H1N2$_{A/Stockholm/15/2014}$, which were infected again on day 28 post prime with the same H1N2 viruses. (b) Homologous NACHO ELISA titer of ferret sera sampled on day 14 after inoculation with H1N2 virus and 2 weeks after the boost with recombinant NA or by re-inoculation with H1N2$_{A/Estonia/91621/2015}$ or H1N2$_{A/Stockholm/15/2014}$ (indicated by arrows on the X-axis). (c) 43 BALB/c mouse immunization and blood sampling scheme. (d) Homologous NACHO serum IgG titers in pooled sera from mice that were immunized twice with recombinant NA. Mouse and ferrets representations were created with BioRender.com (2023).

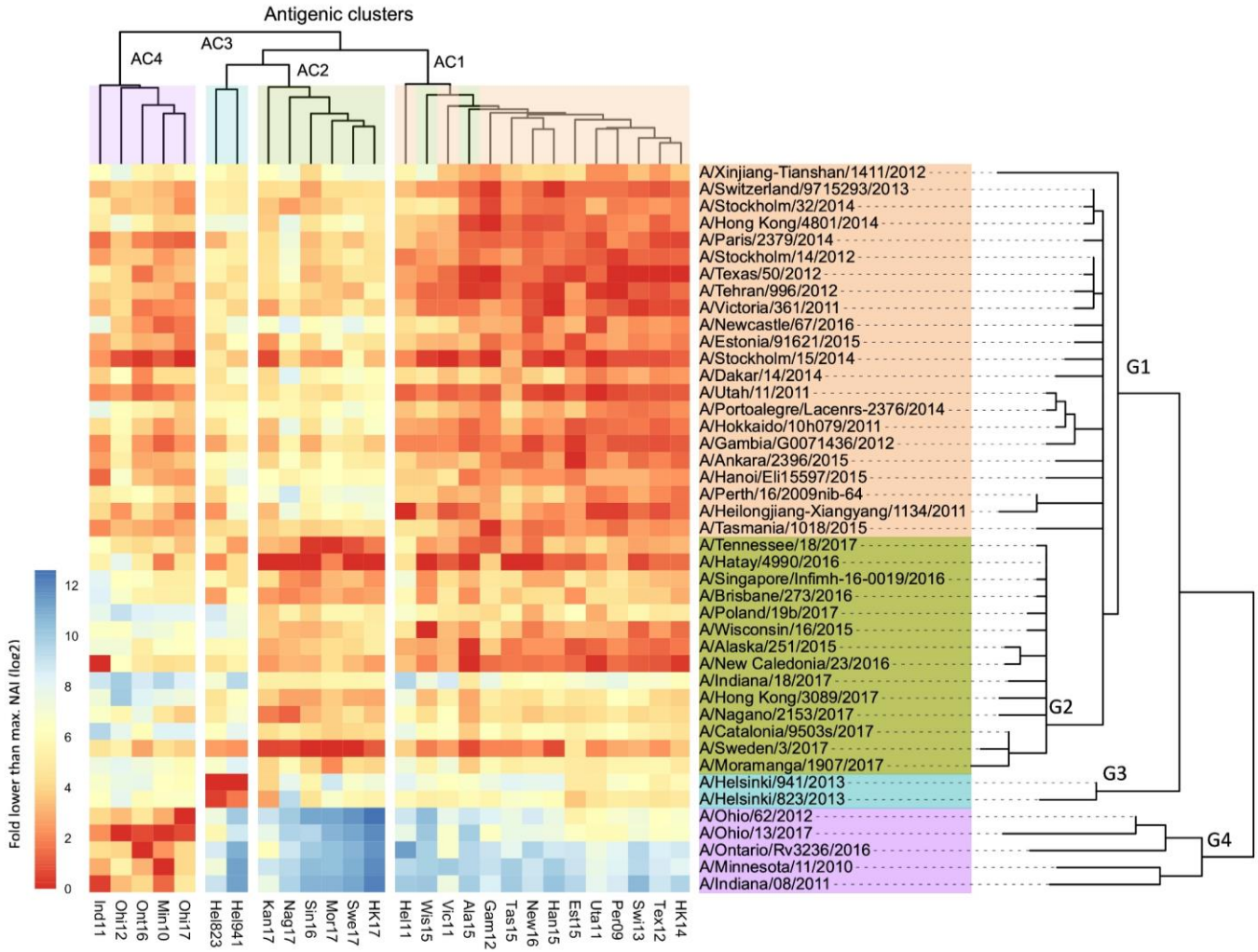

Figure 2. Breadth of N2 NA inhibition. 43 Phylogenetic tree based on the N2 NA head domain amino acid sequences and heat-map representing the average of normalized neuraminidase inhibition per H6N2 [$\log_2$ (max (NAI/ ELISA homologous titer)/(NAI/ homologous ELISA titer)] determined in ferret sera after the boost (listed vertically). The red-to-blue scale indicates high-to-low NAI observed in ELLA against the H6N2 reassortants (listed at the bottom). UPGMA clustering of H6N2s inhibition profiles are shown on top of the heat map and coloured according to the phylogenetic groups.

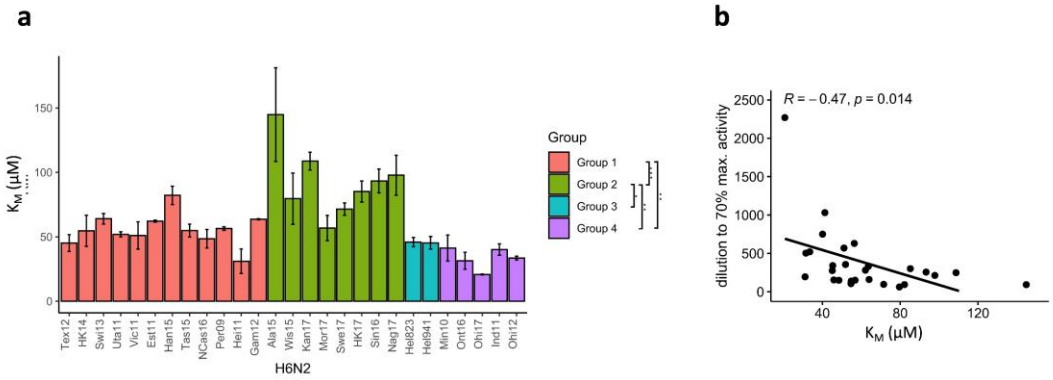

Figure 2. Figure supplement 1. The N2 NA substrate affinity is distinct in the N2 phylogenetic groups. (a) K_M was determined for each H6N2 reassortant virus using the fluorogenic substrate MUNANA. N2 NAs are coloured according to the phylogenetic groups. Global test comparing the 4 groups was done using ANOVA (P= 2.4e-05) and pairwise comparison performed using Wilcoxon, ***P< 0.001, **P< 0.01, *P< 0.05. (b) Scatter-plot and correlation between the K_M values and dilutions required to obtain 70% max activity in ELLA.

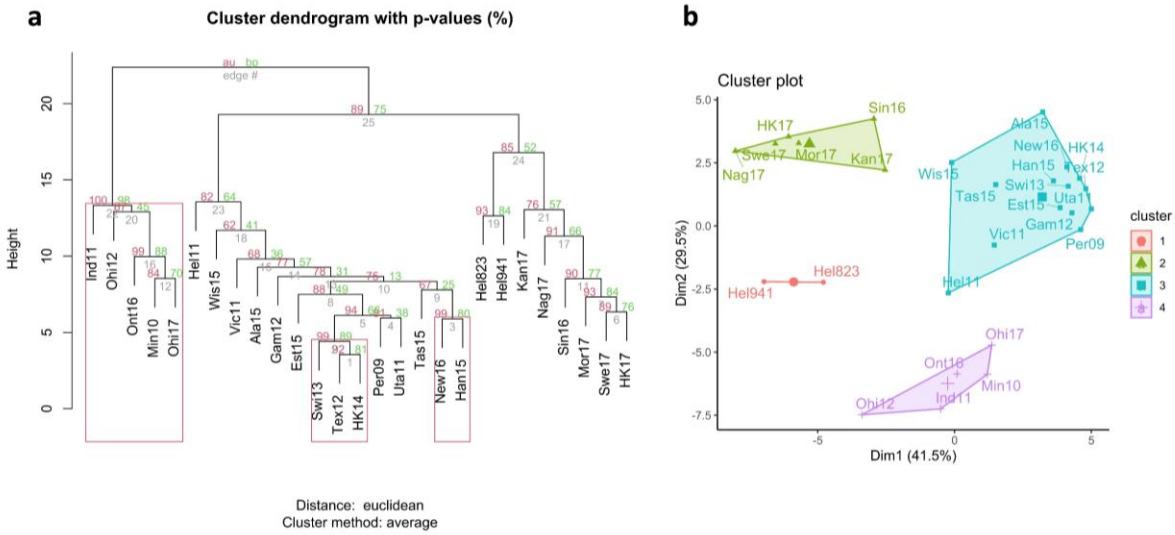

Figure 2. Figure supplement 2. Antigenic relationship between NA of the H6N2 viruses. (a) Hierarchical clustering based on multisampling and multiscale bootstrap resampling. Approximately unbiased p-values (AU) are shown in red, bootstrap values in green, and edge values in grey. The red brackets represent the clusters with AU > 95%. (b) K-means clustering represented using principal component analysis (k=4).

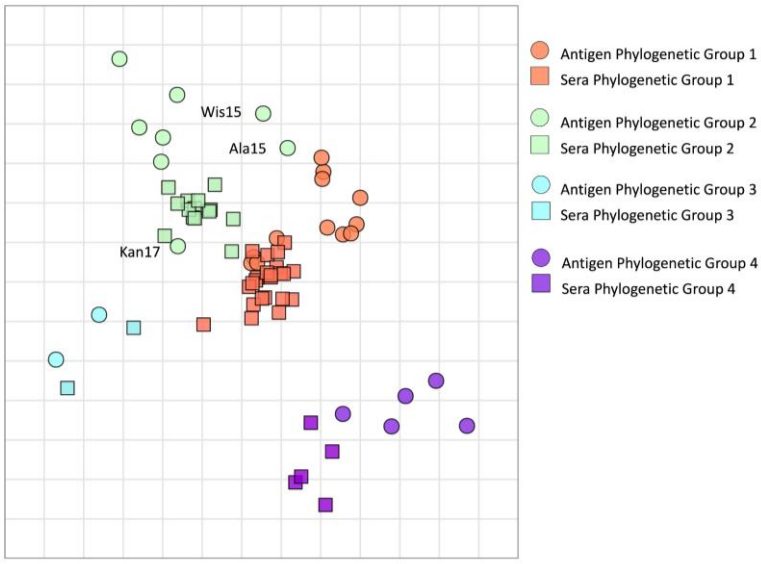

Figure 2. Figure supplement 3. Antigenic map of N2 NAs. Antigen and sera distances are represented in the graph and coloured according to distinct phylogenetic groups. The spacing between grid lines is 1 unit of antigenic distance corresponding to a twofold dilution of immune serum in the NAI assay.

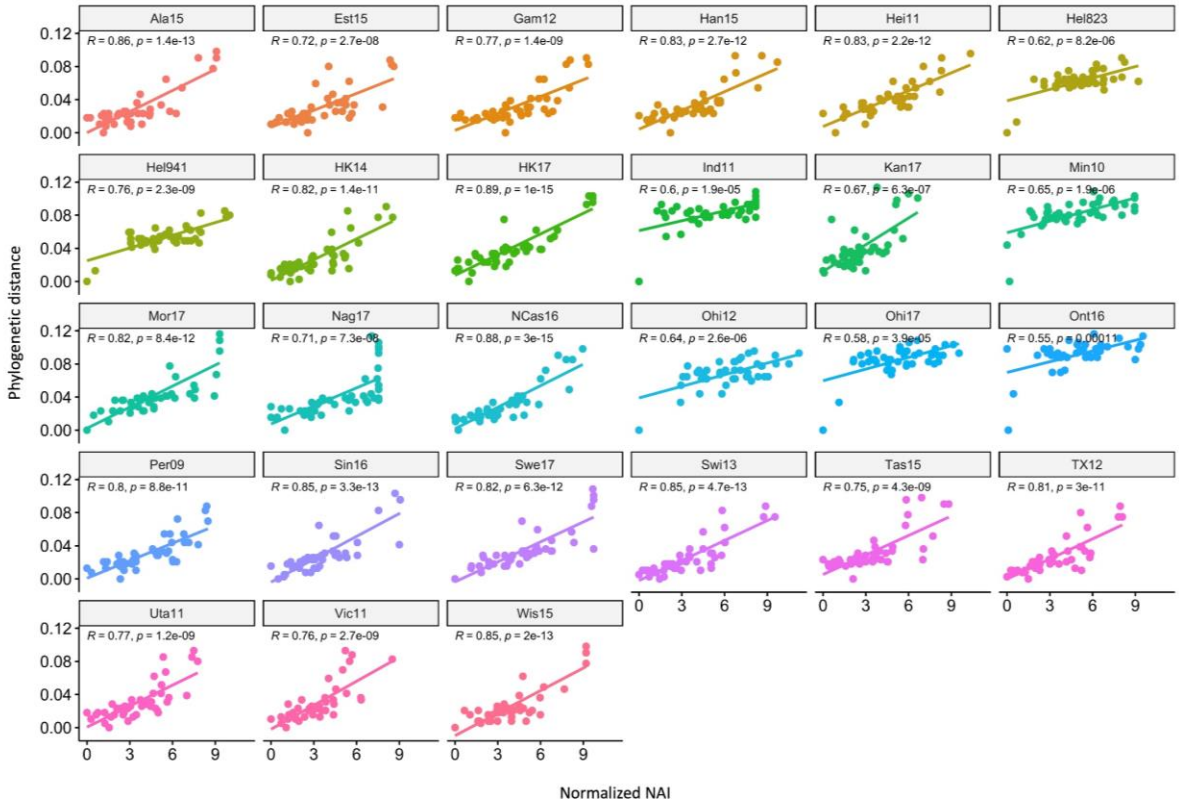

Figure 2. Figure supplement 4. Correlation of NAI fold reduction and phylogenetic relatedness. The scatter plots show the phylogenetic distances (y-axis) and Normalized NAI as fold reduction relative to the maximal inhibition [$\log_2$ (max NAI/NAI)] (x-axis). Each graph represents one of the 27 H6N2s that were tested.

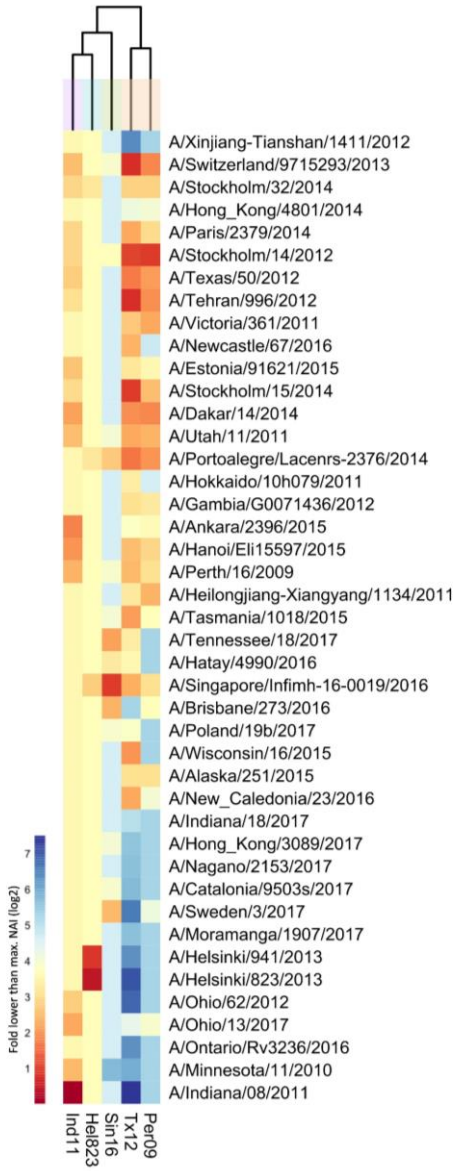

Figure 2. Figure supplement 5. Breadth of N2 inhibition of sera from ferrets primed by H1N2 infection only. 43 Heat-map representing the average of normalized neuraminidase inhibition per H6N2 [$\log_2$ (max NAI/NAI)] determined in ferret sera 2 weeks after infection. The red-to-blue scale indicates the fold reduction compared to the max NAI observed in ELLA against the H6N2 reassortants (listed at the bottom). UPGMA clustering of H6N2 inhibition profiles are shown on top of the heat map and coloured according to the phylogenetic groups.

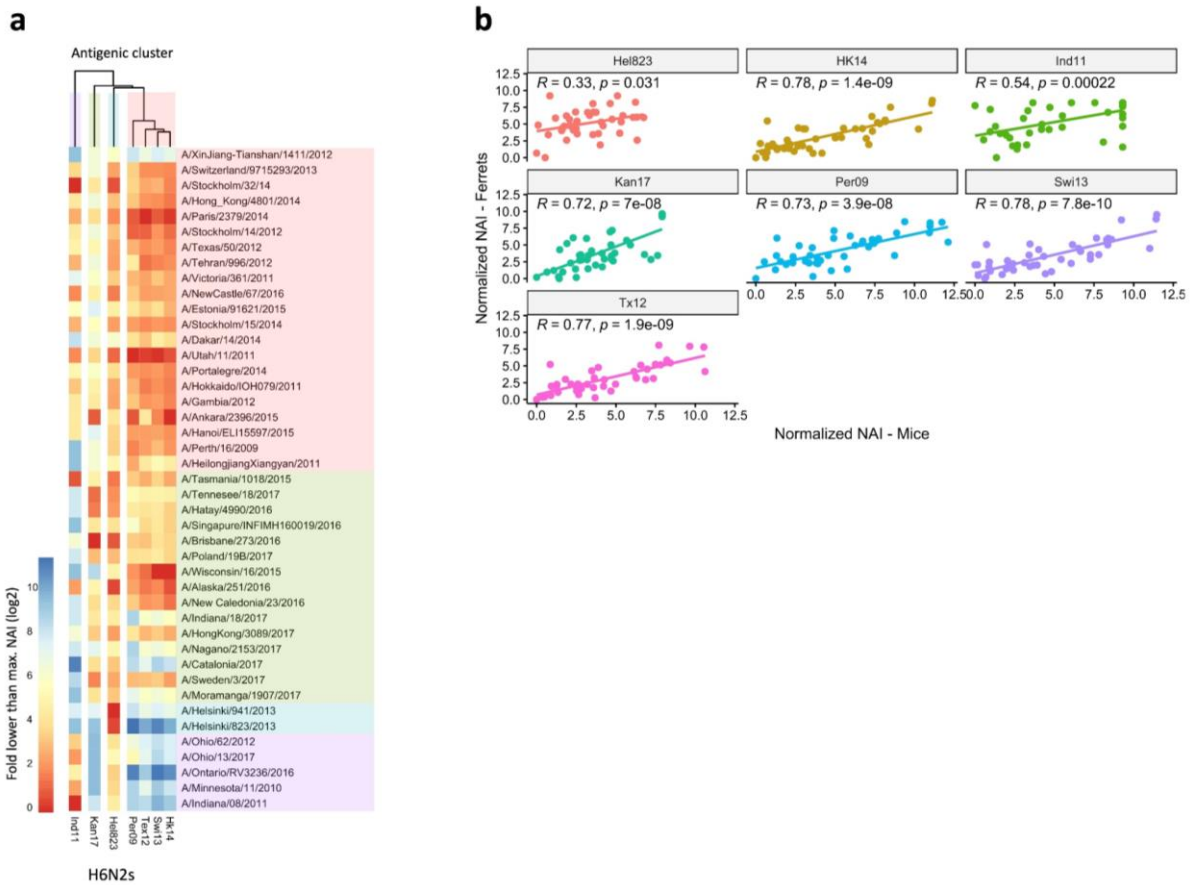

741

742 **Figure 2. Figure supplement 6. Breadth of N2 inhibition is confirmed in mouse sera.** 43 Heat-map representing
743 the average of normalized neuraminidase inhibition per H6N2 [$\log_2$(max NAI/NAI)] determined in mice sera after
744 the boost (listed on the right). The red-to-blue scale indicates low-to-high NAI observed in ELLA against the H6N2
745 reassortants (listed at the bottom). UPGMA clustering of H6N2 inhibition profiles are shown on top of the heat
746 map and coloured according to the phylogenetic groups. (b) **Correlation of NAI between mice and ferrets**.
747 Scatter plot shows the normalized NAI as fold reduction from maximal inhibition [$\log_2$ (max NAI/NAI)] from
748 ferrets (y-axis) versus mice (x-axis). The 7 H6N2s tested are indicated in the graphs.

749

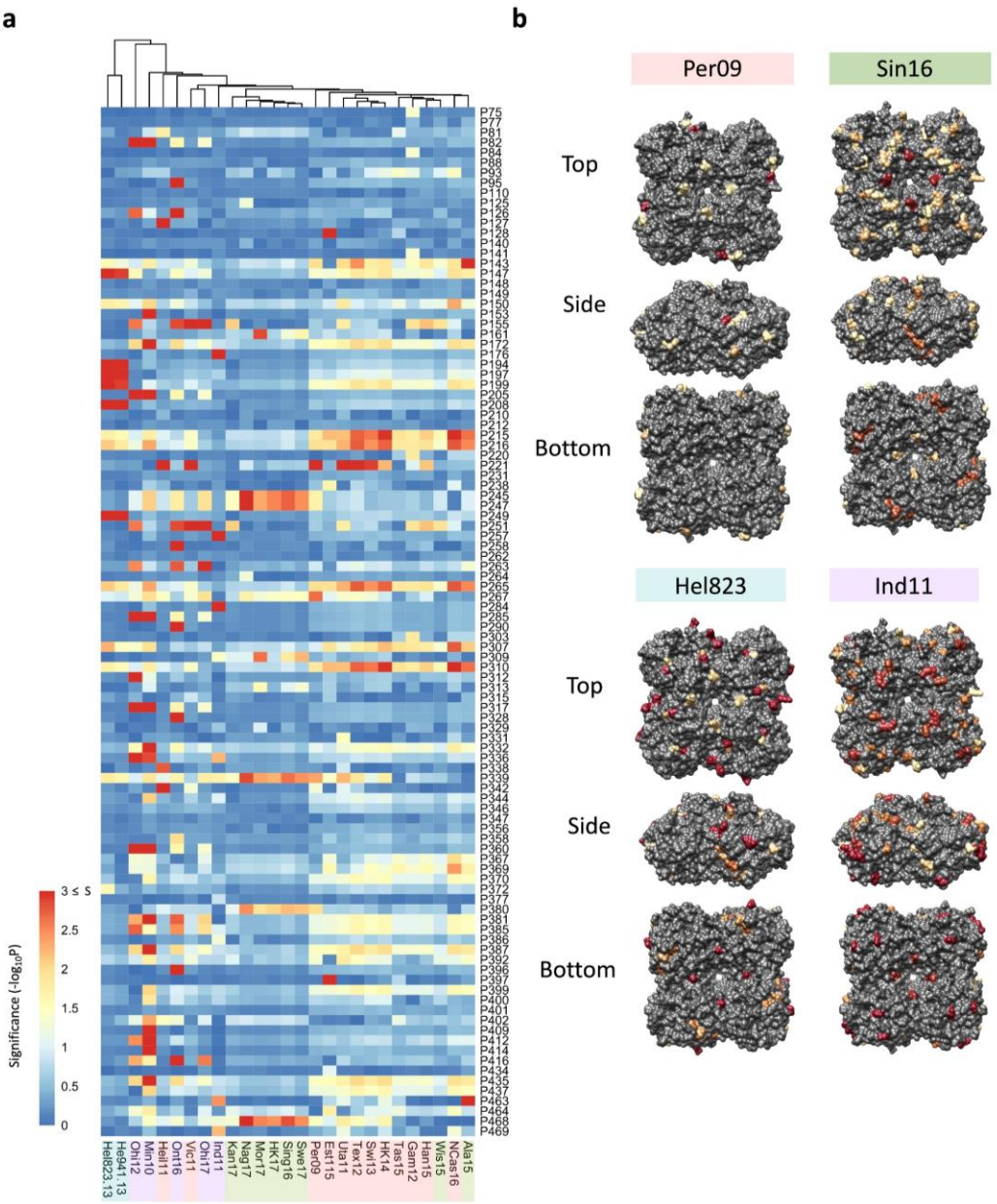

Figure 3. Association analysis reveals impact of amino acid mutations on NAI. (a) Association study performed for each H6N2 virus (listed at the bottom) to determine the probability of each variable amino acid (listed on the right) present in the panel of 43 NAs to impact the NAI. The red-to-blue scale represents significance values ($S=-\log_{10}P$) associated with each amino acid substitution. The dark red in the color scale represent all values that are equal or higher than 3 (corresponding to p-values ≤ 0.001). The colour shades on the bottom side indicate the distinct phylogenetic groups. (b) The significant values ($p<0.05$) were represented on the surface of N2 tetramer (PDB accession number 4H53) for one representative strain of each phylogenetic group with a yellow to red scale of significance ($-\log_{10}P$).

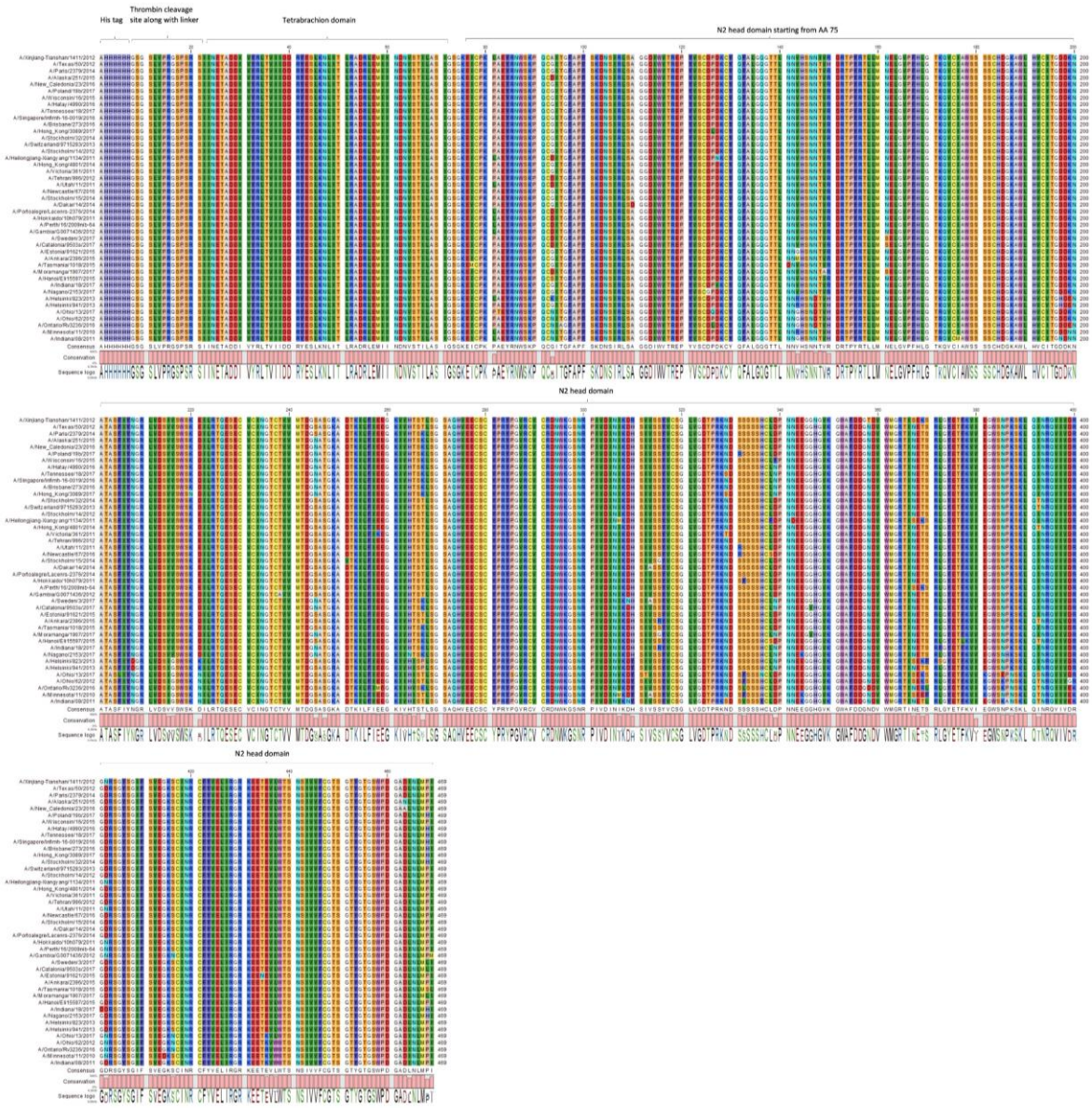

Figure 3 – figure supplement 1. Protein sequence alignment of N2 NACHO panel used for immunization. The sequence of recombinant NA that was used for boosting ferrets or to prime/boost BALB/c mice was aligned starting from the HIS-tag, tetrabrachion and followed by NA head domain, as depicted on top of the sequences.

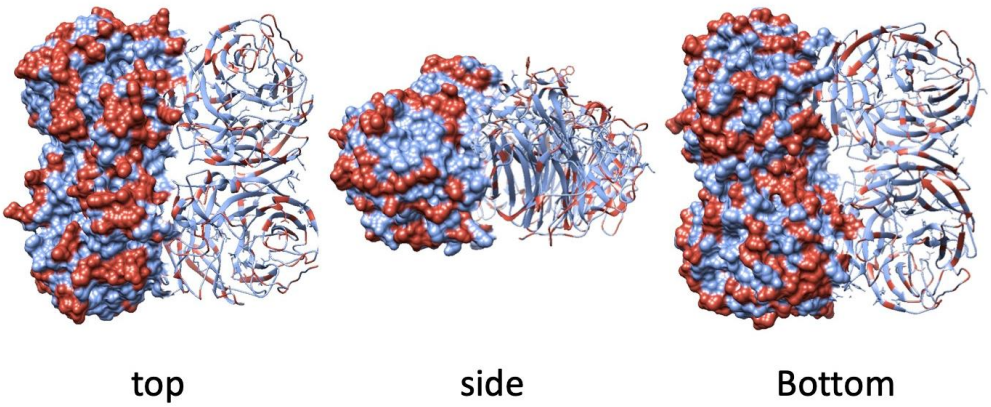

Figure 3 – figure supplement 2. Geometrical distribution of amino acid substitutions in the N2 structure. The surface and ribbon representation indicate the geometrical distribution of the amino acid substitutions that are present in the panel of 43 N2 NAs used as immunogens in the study. Substitutions are highlighted in red on the model structure of N2 from H2N2 (A/RI/5+/1957, PBD 4H53).

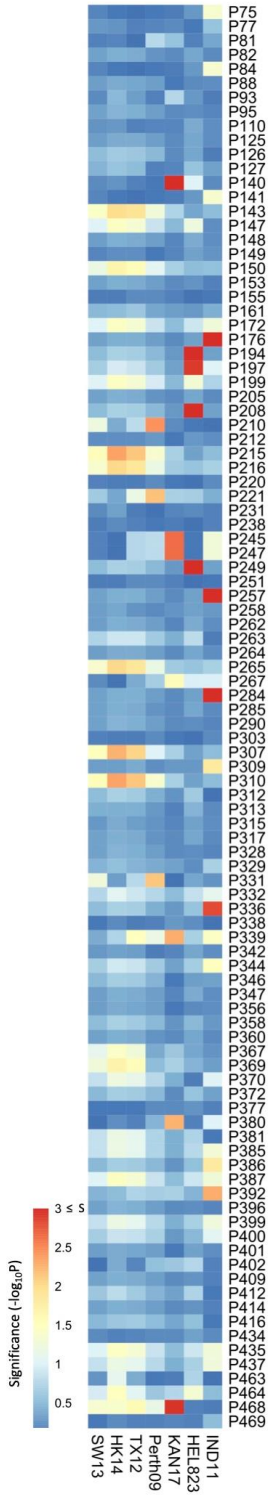

Figure 3 – figure supplement 3. Association study was performed on data obtained from mouse sera. (a) Association study performed for each H6N2 virus (listed at the bottom) to determine the probability of each variable amino acid (listed on the right) present in the panel of 43 NAs to impact NAI. The red-to-blue scale represents significance values (-$\log_{10}$P) associated with each variable amino acid.

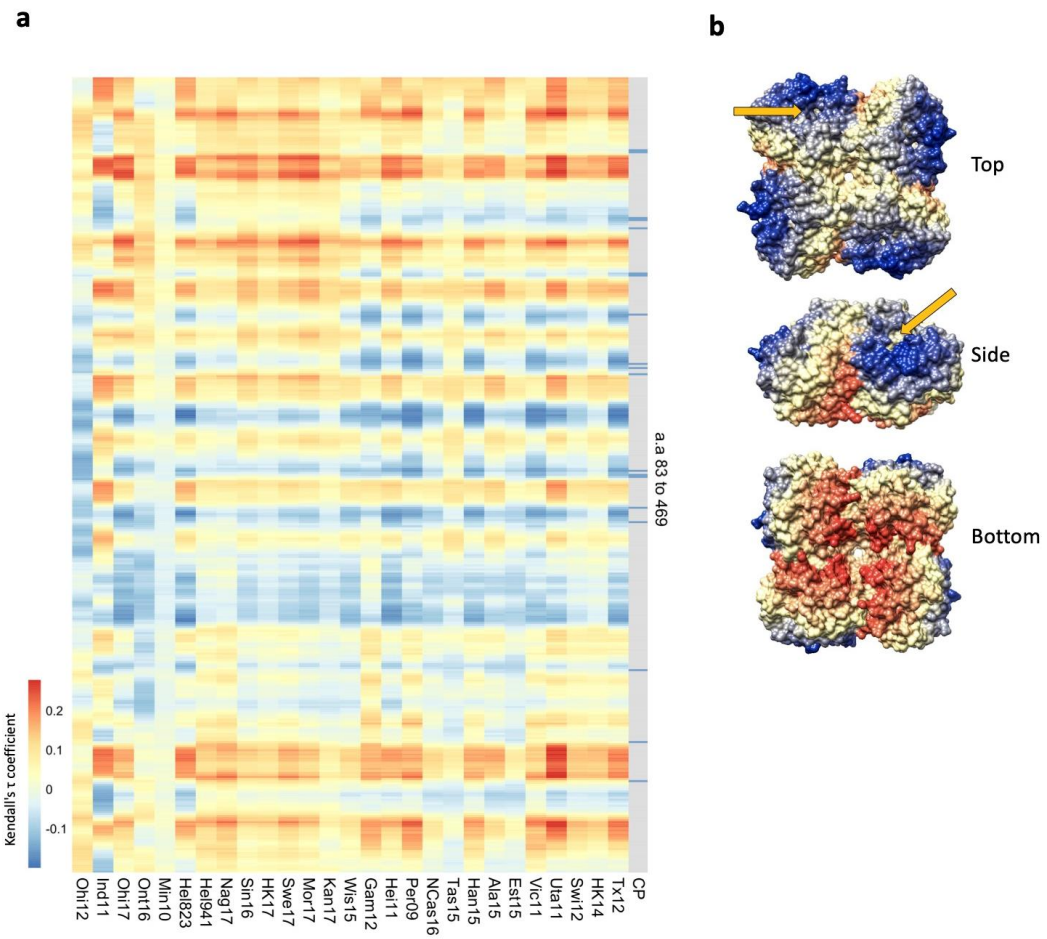

Figure 4. Residues close to the catalytic pocket are more likely to impact NAI. (a) Significance values (102 variable amino acids) obtained from the association study were correlated to the distance between every amino acid and each of the variable amino acids in the NA structure. The red-to-blue scale represents the Tau values obtained in the Kendall correlation. Amino acids 83 to 469 are shown from top to bottom in the heatmap. The H6N2s used in the NAI panel are listed at the bottom. The grey column indicates the residues that are part of the catalytic pocket (CP) that directly interact with the substrate (R118, D151, R152, R224, E276, R292, R371, and Y406) and the residues that play a key role in stabilizing the catalytic site (E119, R156, W178, S179, D198, I222, E227, H274, E277, N294, and E425). (b) Tau values obtained from Tex12 H6N2 correlation are represented on the surface of the N2 structure of A/RI/5+/1957 (PBD 4H53), the arrow indicates the catalytic pocket in one NA protomer.

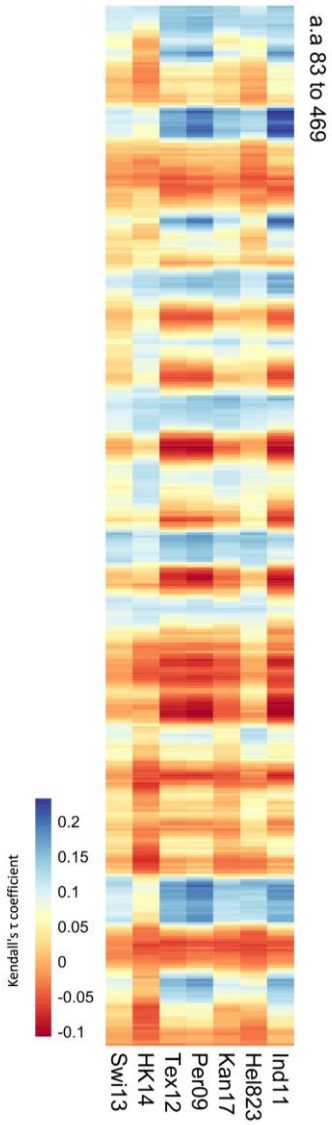

Figure 4 – figure supplement 1. Correlation of values obtained from the mouse sera panel and amino acid distances. (a) Significance values (102 variable amino acids) obtained from the association study were correlated to the distance between every amino acid and each of the variable amino acids in the NA structure. The red-to-blue scale represents the Tau values obtained in the Kendall correlation. Amino acids 83 to 469 are shown from top to bottom of the heatmap. The H6N2s used in the NAI panel are listed at the bottom.

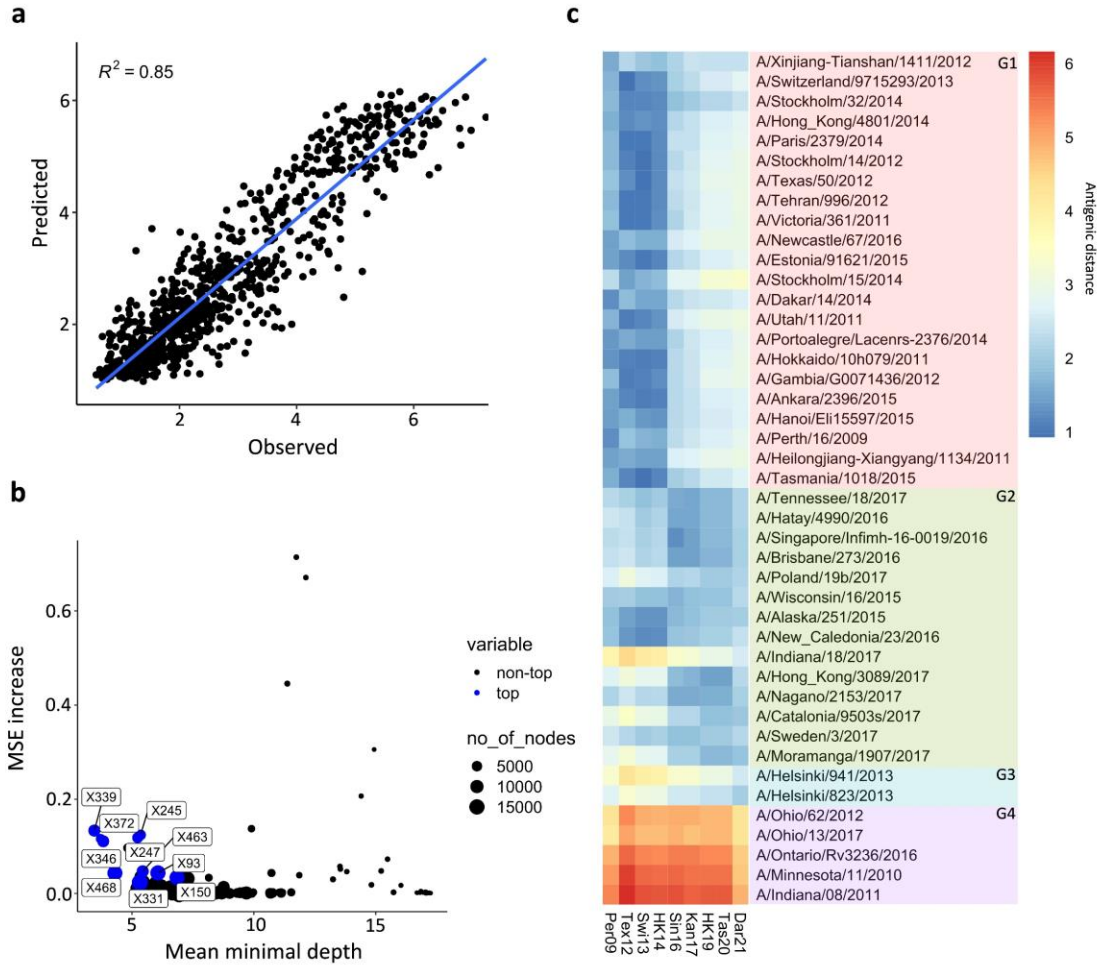

Figure 5. Prediction of N2 antigenicity based on machine learning. (a) Predicted *vs* observed normalized NAIs are shown. (b) Multi-way importance plot indicating the increase in mean standard error, the mean depth, and number of nodes. The top 10 most important amino acid changes are highlighted in blue and annotated with their position in the NA sequence. (c) 43 The heatmap indicates the predicted antigenic distances of N2s from recent H3N2 isolates (at the bottom of the heatmap) relative to the N2s that were used in the NAI breadth panel (listed vertically). The antigenic distances were calculated based on NA protein sequence.